TKK Dissertations 260
Espoo 2010

MODELING MATERIALS WITH PHASE FIELD CRYSTAL MODELS

Doctoral Dissertation

Akusti Jaatinen

Aalto University
School of Science and Technology
Faculty of Information and Natural Sciences
Department of Applied Physics

TKK Dissertations 260
Espoo 2010

MODELING MATERIALS WITH PHASE FIELD CRYSTAL MODELS

Doctoral Dissertation

Akusti Jaatinen

Doctoral dissertation for the degree of Doctor of Science in Technology to be presented with due permission of the Faculty of Information and Natural Sciences for public examination and debate in Auditorium K at the Aalto University School of Science and Technology (Espoo, Finland) on the 17th of December 2010 at 13 o'clock.

Aalto University
School of Science and Technology
Faculty of Information and Natural Sciences
Department of Applied Physics

Aalto-yliopisto
Teknillinen korkeakoulu
Informaatio- ja luonnontieteiden tiedekunta
Teknillisen fysiikan laitos

Distribution:
Aalto University
School of Science and Technology
Faculty of Information and Natural Sciences
Department of Applied Physics
P.O. Box 11100 (Otakaari 1 M)
FI - 00076 Aalto
FINLAND
URL: http://tfy.tkk.fi/
Tel. +358-9-47001
E-mail: Akusti.Jaatinen@tkk.fi

ISBN 978-952-60-3518-5
ISBN 978-952-60-3519-2 (PDF)
ISSN 1795-2239
ISSN 1795-4584 (PDF)
URL: http://lib.tkk.fi/Diss/2010/isbn9789526035192/

TKK-DISS-2854

Picaset Oy
Helsinki 2010

Aalto University

ABSTRACT OF DOCTORAL DISSERTATION	AALTO UNIVERSITY SCHOOL OF SCIENCE AND TECHNOLOGY P.O. BOX 11000, FI-00076 AALTO http://www.aalto.fi

Author Mikko Akusti Jaatinen

Name of the dissertation

Modeling materials with phase field crystal models

Manuscript submitted 26.10.2010	Manuscript revised 30.11.2010
Date of the defence 17.12.2010	
☐ Monograph	☒ Article dissertation (summary + original articles)

Faculty	Faculty of Information and Natural Sciences
Department	Department of Applied Physics
Field of research	F039Z Theoretical and computational physics (Tfy-105)
Opponent(s)	Prof. John Lowengrub (Univ. California at Irvine)
Supervisor	Prof. Tapio Ala-Nissilä
Instructor	Prof. Tapio Ala-Nissilä, Prof. Seppo Louhenkilpi and Prof. Ken Elder (Oakland Univ.)

Abstract

The phase field crystal (PFC) model is a novel approach for modeling phenomena on atomistic length and diffusive time scales. In this dissertation, we present new advances in the methodology of the PFC model and describe applications to solidification and grain boundaries. We present an extended phase diagram for the original formulation of the PFC model that allows to model three dimensional hexagonal and cubic close-packed crystal structures. The original PFC model is also applied to study crystallization of different polymorphs in diffusion-controlled growth. We also study the connection between the PFC model and statistical mechanical density functional theory of classical systems. Based on these studies, we propose a new variant of the PFC model. We show that using our new formulation of the model, it is possible to reproduce certain static and dynamic properties of the density functional theory with significantly greater accuracy than with previously proposed PFC models without losing the numerical feasibility of the PFC model. The new PFC model is applied to study grain boundaries of body-centered cubic iron near its melting point.

Keywords phase field crystal, density functional theory of classical systems, crystal growth	
ISBN (printed) 978-952-60-3518-5	ISSN (printed) 1795-2239
ISBN (pdf) 978-952-60-3519-2	ISSN (pdf) 1795-4584
Language English	Number of pages 70 p. + app. 50 p.
Publisher Aalto University School of Science and Technology, Department of Applied Physics	
Print distribution Aalto University School of Science and Technology, Department of Applied Physics	
☒ The dissertation can be read at http://lib.tkk.fi/Diss/2010/isbn9789526035192/	

Aalto-yliopisto

VÄITÖSKIRJAN TIIVISTELMÄ	AALTO-YLIOPISTO TEKNILLINEN KORKEAKOULU PL 11000, 00076 AALTO http://www.aalto.fi

Tekijä Mikko Akusti Jaatinen

Väitöskirjan nimi

Materiaalien mallintaminen faasikenttäkidemalleilla

Käsikirjoituksen päivämäärä 26.10.2010	Korjatun käsikirjoituksen päivämäärä 30.11.2010
Väitöstilaisuuden ajankohta 17.12.2010	
☐ Monografia	☒ Yhdistelmäväitöskirja (yhteenveto + erillisartikkelit)

Tiedekunta	Informaatio- ja luonnontieteiden tiedekunta
Laitos	Teknillisen fysiikan laitos
Tutkimusala	F039Z Teoreettinen ja laskennallinen fysiikka (Tfy-105)
Vastaväittäjä(t)	Prof. John Lowengrub (Univ. California at Irvine)
Työn valvoja	Prof. Tapio Ala-Nissilä
Työn ohjaaja	Prof. Tapio Ala-Nissilä, Prof. Seppo Louhenkilpi ja Prof. Ken Elder (Oakland Univ.)

Tiivistelmä

Faasikenttäkidemalli (engl. phase field crystal, PFC) on uusi materiaalitieteen mallinnusmenetelmä, jonka avulla voidaan mallintaa prosesseja, jotka tapahtuvat atomistisella mittakaavalla ja diffusiivisella aikaskaalalla. Tässä väitöskirjatyössä on sekä kehitetty PFC-mallin metodologiaa että sovellettu sitä jähmettymisen ja raerajojen mallintamiseen. Esitämme PFC-mallin aluperäiselle muodolle laajennetun faasidiagrammin, jonka avulla mallia voidaan soveltaa tiivispakkauksellisen kuutiollisen ja heksagonaalisen hilarakenteen mallintamiseen. Alkuperäistä PFC-mallia sovelletaan myös saman aineen eri kidemuotojen kasvunopeuksien tutkimiseen diffuusion kontrolloimassa kasvumoodissa. Tutkimme myös PFC-mallin yhteyttä tilastolliseen mekaniikkaan perustuvaan klassillisten systeemien tiheysfunktionaaliteoriaan. Näihin tutkimuksiin perustuen esitämme uuden version PFC-mallista. Näytämme, että uusi mallimme pystyy toistamaan tiettyjä tiheysfunktionaaliteorian staattisia ja dynaamisia ominaisuuksia huomattavasti paremmalla tarkkuudella kuin aiemmin esitellyt PFC-mallit uhraamatta alkuperäisen PFC-mallin numeerista tehokkuutta. Sovellamme uutta PFC-mallia myös tilakeskeisen kuutiollisen raudan raerajojen tutkimiseen sulamispisteen läheisyydessä.

Asiasanat faasikenttämallinnus, klassillinen tiheysfunktionaaliteoria, kiteenkasvu

ISBN (painettu) 978-952-60-3518-5	ISSN (painettu) 1795-2239
ISBN (pdf) 978-952-60-3519-2	ISSN (pdf) 1795-4584
Kieli Englanti	Sivumäärä 70 s. + liit. 50 s.

Julkaisija Aalto-yliopiston teknillinen korkeakoulu, Teknillisen fysiikan laitos

Painetun väitöskirjan jakelu Aalto-yliopiston teknillinen korkeakoulu, Teknillisen fysiikan laitos

☒ Luettavissa verkossa osoitteessa http://lib.tkk.fi/Diss/2010/isbn9789526035192/

Preface

The work presented in this thesis has been carried out in Multiscale Statistical Physics group of Aalto University School of Science and Technology. The group is also a part of Academy of Finland's COMP (Computational Nanoscience) Center of Excellence. I am very grateful for my supervisor, Prof. Tapio Ala-Nissilä, for giving me the opportunity to carry out doctoral studies as a part of his group. Especially I want to thank Tapio for being supportive of my ideas, often motivating me to push them further. I am also very grateful to all the people who I collaborated with in the process of doing the research reported in this thesis. I want to thank Prof. Ken Elder for introducing me the Phase field crystal model, helping me to process my ideas further and reassuring me that the work I've been doing is important. I want to thank my former office mate, Dr. Cristian Achim, for the invaluable help he provided me in so many technical issues. Prof. Laszlo Gránásy and his group deserve many thanks for our fruitful collaboration that led to Publication II. Prof. Seppo Louhenkilpi deserves thanks for all the inspiring discussions about practical applications of mathematical models that we've had over the years.

I also want to thank all my office mates, family and friends, who are too numerous to be listed by names here. Although most of you haven't directly contributed in this work, all the diverting discussions and other activities we've had together during these years have helped me a lot in keeping my motivation up. I know this is the part where I'm suppose to say that I couldn't have finished this thesis without you. As an objective scientist, I'm not sure I can say such thing with certainty. What I can say with high confidence is that if I had to complete this job without having you around, I would have become insane by now. The greatest thanks for my sanity of course belong to my dear wife Lissu, who has always been there for me, even during the few times that this work pushed me to the limits. So truly, with all my heart: Thanks.

Contents

List of Publications

This thesis consists of an overview and of the following publications which are referred to in the text by their Roman numerals.

I A. Jaatinen and T. Ala-Nissila, *"Extended phase diagram of the three-dimensional phase field crystal model,"* Journal of Physics: Condensed Matter **22** 205402 (2010)

II G. Tegze, L. Gránásy, G. I. Tóth, F. Podmaniczky, A. Jaatinen, T. Ala-Nissila and T. Pusztai, *"Diffusion-controlled anisotropic growth of stable and metastable crystal polymorphs in the phase-field crystal model,"* Physical Review Letters **103**, 035702 (2009)

III A. Jaatinen, C. V. Achim, K. R. Elder, and T. Ala-Nissila, *"Thermodynamics of bcc metals in phase-field-crystal models,"* Physical Review E **80**, 031602 (2009)

IV A. Jaatinen, C. V. Achim, K. R. Elder and T. Ala-Nissila, *"Phase field crystal study of symmetric tilt grain boundaries of iron,"* Technische Mechanik **30**, 169-176 (2010)

V A. Jaatinen and T. Ala-Nissila, *"Eighth-order phase-field-crystal model for two-dimensional crystallization,"* Physical Review E, accepted for publication

Author's contribution

The author has had an active role in all phases of the research reported in this thesis. He has written the first drafts of publications I, III, IV and V. Publications I and V are based on calculations and their interpretations by the author. In Publication II, the author's role was defining the thermodynamical driving forces for each phase studied. Publication III is based on calculations and their interpretations by the author, except for the grain boundary energies. In Publication IV interpretation of the results was done by the author.

List of Abbreviations

BCC	Body-centered cubic
BCT	Body-centered tetragonal
CDFT	Classical density functional theory
CSL	Coincidence site lattice
DDFT	Dynamical density functional theory (of classical systems)
EOF	Eighth-order fit
FCC	Face-centered cubic
FOF	Fourth-order fit
GBE	Grain boundary energy
HCP	Hexagonal close-packed
MD	Molecular dynamics
PF	Phase field
PFC	Phase field crystal
RY	Ramakrishnan and Yussouff
SH	Swift and Hohenberg
WK	Wu and Karma

List of Symbols

$S(k)$	Structure factor
k	Length of a wave vector
k_m	Position of the main peak in $S(k)$
$\phi(\mathbf{r})$	Phase field variable
$\mathbf{r}$	Spatial coordinate
t	Time
M	Mobility
F	Free energy
α, λ, q_0, h, g	Parameters of the Swift-Hohenberg PFC model
$\mathbf{x}$	Rescaled spatial coordinate
ϵ	Rescaled parameter of the Swift-Hohenberg PFC model
ψ	Dimensionless phase field variable
$\tilde{F}$	Rescaled free energy
τ	Rescaled time variable
ψ_0	Spatial average of ψ
u	Amplitude of density fluctuations
q	Wave vector corresponding to density fluctuations
a_l	Lattice spacing
x	Position of a moving solid-liquid interface
d	Growth velocity parameter for diffusion controlled growth
Ω	Grand potential
$\mu_{int}(\mathbf{r})$	Intrinsic chemical potential
μ	Chemical potential
$u(\mathbf{r})$	External potential energy field
$\rho(\mathbf{r})$	One-particle density
$\mathcal{F}$	Intrinsic free energy
k_B	Boltzmann's constant

T	Absolute temperature
λ_T	Thermal de Broglie wavelength
$c^{(n)}(\mathbf{r}_1 \dots \mathbf{r}_n; \rho_0)$	n-body direct correlation function
ρ_0	Reference density
β	Thermodynamic beta
$h(r)$	Total pair correlation function
r	Length of a spatial coordinate vector
$\Delta\rho^*$	Fractional density change in freezing
$\mathbf{G}$	Reciprocal lattice vector
$\mu_{\mathbf{G}}$	Amplitude of Fourier mode corresponding to $\mathbf{G}$
γ	Friction coefficient
$\mathbf{F}$	Potential force
$\mathbf{f}$	Gaussian random force
n	Dimensionless density variable
$\bar{\rho}$	Spatial average of $\rho(\mathbf{r})$
$C(r)$	Reference density times two-body direct correlation function
E_S	Expansion parameter in fourth- and eighth-order expansions of $\hat{C}(k)$
a, b	Parameters for local part of free energy in DFT-based PFC models
E_B	Expansion parameter in eighth-order expansion of $\hat{C}(k)$
θ	Misorientation angle of a grain boundary
$w(r)$	Weighing function
ρ_s, ρ_l	Densities of solid and liquid phases at coexistence
ρ_i	Initial density
Δ	Undercooling
v	Velocity of a solid-liquid interface
D	Effective diffusion coefficient
$\mathcal{L}$	Linear part of time-evolution operator
$\mathcal{N}$	Non-linear part of time-evolution operator
$\mathfrak{F}, \mathfrak{F}^{-1}$	Forward and inverse Fourier transform operators

List of Figures

List of Tables

1 Introduction

Formation of a solid phase, when a liquid is cooled below its freezing point, is such a matter of course in everyday life that one seldom wonders what exactly happens during the process and why. Therefore, it might be surprising to learn that even today finding more accurate answers to these very questions are of great importance to both academic and industrial communities. From a scientific point of view, even though the basic principles of why solidification emerges are known, many details about the process still lack an adequate explanation. From a technological standpoint, more accurate understanding of solidification is desired for at least two important reasons. First, the details of the process through which a material is prepared greatly affect the microstructure of the material. Therefore a more detailed understanding of solidification processes could potentially enable one to manufacture materials with better properties. Second, if the processes involved in solidification were known more accurately, the knowledge could potentially be utilized in manufacturing new kinds of self-organizing nanostructures.

First mathematical descriptions of solidification date back to 1831, when French scientists Gabriel Lamé and Benoît Paul Émile Clapeyron studied the thickness of a solidifying crust on top of a liquid as a function of time. Later in about 1890, a similar equation of motion for the boundary between the phases was formulated by a Slovene physicist Jožeph Stefan (best known for the Stefan-Boltzmann radiation law) for studying the formation of ice in the polar seas. [1] After Stefan, the class of mathematical problems that consider a moving sharp interface between two phases are known as Stefan problems. In Stefan problems, the solid and liquid phases are treated as continuous matter, with a sharp interface separating the two phases. The formulations take into account the known laws of energy conservation and heat transport, and their effect on the motion of the interface. Progress on mathematical formulations and solutions to the continuum sharp-interface Stefan problems has

continued throughout the 20$^{\text{th}}$ century [1, 2].

Starting from the mid-1980s, another continuum approach to modeling solidification known as phase field (PF) models emerged. The method was motivated in part by Hilliard and Cahn's work on the interface between a solid and its melt [3], as well as numerical feasibility. The most profound difference between PF models and Stefan problems is that, in PF models, the explicit tracking of solid and liquid phases and the interface in between is replaced by a continuous order parameter field. This field exhibits constant values in the bulk of solid and liquid phases (for example, one in the solid and zero in the liquid), and a smooth transition between the two values in the boundary between the phases. Due to the smooth, rather than sharp, interface between the solid and liquid phases, the PF models are also known as the diffuse interface approach to modeling solidification. The most important advantage of PF models over more traditional Stefan approaches is that it allows the study of much more complicated solidification patterns, as one does not need to explicitly track the position of the interface (see e.g. Ref. [4] for a brief and recent review of PF models and their applications in materials science, or Ref. [5] for a more thorough introduction to the subject).

On the other hand, as the atomistic view of the world developed in the 20$^{\text{th}}$ century, the question of how the transition between solid and liquid phases emerges from the laws governing the motions of individual atoms began to draw attention. As early as 1910, the first theory explaining mechanism of melting was proposed by Lindemann, who used vibration of atoms in the crystal to explain the melting transition. Based on his model, Lindemann proposed a simple criterion stating that melting of a solid would be expected, when amplitude of the lattice vibrations reaches about 10 % of the nearest-neighbor distance [6]. In subsequent studies this criterion, now known as the Lindemann melting rule, has been found to agree well with experiments for many simple solids (see for example Ref. [7]). In another approach in 1969, starting from the liquid side, Hansen and Verlet found from computer simulations of the Lennard-

Jones system that freezing of the liquid occurs when the height of the first peak in the dimensionless structure factor $S(k_m)$ of the liquid, a measure of the degree of long-range order in the liquid, reaches a value of 2.85 [8]. In subsequent studies, it has been generalized that freezing of simple liquids takes place when $S(k_m) \simeq 2.9 \pm 0.1$, and the rule has now become known as the Hansen-Verlet freezing criterion [9].

The foremost classical theory of freezing that could explain both of the above mentioned empirical rules is the classical density functional theory (CDFT) of freezing, proposed by Ramakrishnan and Yussouff (RY) in 1979 [10]. The theory of RY uses the structure factor $S(k)$ of the liquid as an input, from which it predicts a periodic density profile of a solid phase, and then defines whether this solid coexists with the liquid. In their study of argon and sodium, RY showed that using their theory the requirement for $S(k_m)$ to obtain a coexistence between solid and liquid phases agreed quantitatively with the Hansen-Verlet melting rule. In addition the predicted density profiles of the solid agreed well with the Lindemann melting criterion. After RY, the CDFT of freezing has been extended and applied to study a wide range of phenomena including the freezing of various different fluids, solid-melt interfaces, nucleation, and binary mixtures and more complex materials (see Ref. [9] and references therein). The theory has also been refined and many variants have been proposed, perhaps the most sophisticated variant to date being the fundamental measure theory, which is able to predict freezing properties of hard objects with a remarkable accuracy [11].

The phase field crystal (PFC) model, which is a central topic of the present work, was developed by K. R. Elder *et al.* as recently as 2002 [12]. The PFC model, which shares many features with the CDFT of freezing, was presented as an extension of the PF models to study phenomena taking place on smaller length scales. The most prominent difference between the PFC and PF models is that in PFC the order parameter field, which is constant in the bulk of the solid in the PF approach, is replaced by a field that exhibits the periodic crystal structure of the solid

phase [12, 13]. Emergence of the PFC model has stimulated rapid progress in the understanding of microscopic phenomena involved in solidification and many other processes, as it allows the study of phenomena taking place on atomistic length and diffusive time scales, the combination of which remains inaccessible for molecular dynamics (MD) simulations using present-day computers. Indeed, the PFC model has already proven itself useful in modeling various phenomena, including elastic and plastic deformation of materials [13, 14, 15], dislocation dynamics [16], crystal growth [17], grain boundary premelting [18, 19] and static and dynamic properties of driven layers [20, 21, 22, 23].

One of the practical challenges to PFC has been modeling different close-packed crystal structures. Because it was for long believed that in its original form the PFC model would not show stable close-packed crystal structures, some ad-hoc modifications to the free energy functional have been proposed in the literature [24, 25]. In the present work, we carry out a numerical calculation of the extended phase diagram of the original PFC model that reveals that the 3D close-packed hexagonal and cubic structures are in fact stable in a certain parameter range of the model. We also apply the original model to study the kinetics and anisotropy of diffusion controlled growth of different crystal polymorphs.

In addition to its practical ability in modeling phenomena on atomistic length and diffusive time scales, bridging the gap between atomistic and continuum modeling methods, the PFC is also an important theoretical construct in bridging together the approaches of CDFT of freezing and PF modeling. Due to the periodic nature of the order parameter field in the PFC model, it is not difficult to come up with an intuitive interpretation that the field must be related to the probability density of finding an atom. Therefore, it is reasonable to assume that the PFC model could be derived from CDFT. As it is possible to obtain refined versions of the PF models from the PFC models in so-called amplitude extension approaches [26, 27, 28, 29, 30, 31], establishing a connection between CDFT and PFC models would close the chain

from classical first principles theories to PF models. In addition it would provide means for systematically selecting the parameters in the PFC model in such a way that certain quantitative properties of a given material could be incorporated in the model.

The first attempt to establish the connection between CDFT and PFC was presented in 2007 by Elder *et al.* [32]. They showed that assuming the field defined within the PFC model is linearly proportional to the atomic density in CDFT, the PFC model can be viewed as a simplified version of CDFT. Wu and Karma [33] introduced another way of obtaining the parameters for the PFC model using a CDFT-like approach. In the present work, we identify the strengths and weaknesses of the approaches proposed in Refs. [32] and [33]. In addition, we propose a new variant of the PFC model known as the eighth-order fit (EOF), which is shown to reproduce certain thermodynamic properties of the material under study significantly more accurately than the previously proposed methods. The EOF model is successfully applied to study grain boundary energies of body-centered-cubic iron. We also present an alternative interpretation of the field within the EOF model, which relates it to the physical atomic density through a convolution. This allows us to derive the free energy of the EOF model in a way which we believe is more consistent with CDFT than the previously presented derivations. Predictions of the EOF model for crystal growth velocities are tested against a dynamical extension of CDFT, as well as other related PFC models. Over all, the results we obtain from the EOF model are very promising. Therefore we believe the current work has both built up the theoretical foundation of the PFC models, as well as provided the community of PFC modeling with means to model certain materials with quantitative accuracy.

2 Phase field crystal model

The phase field crystal (PFC) model can be used for modeling crystallization and many other materials science phenomena taking place at atomistic length and diffusive time scales. Various applications, including crystal growth [17], grain boundary premelting [18, 19], elastic and plastic deformation of materials [13, 14, 15], dislocation dynamics [16], and the effect of an external force on two-dimensional layers [20, 21, 22], have been presented in the scientific literature. The greatest advantage of the PFC model over traditional phase field models is that because the order parameter field exhibits the crystal symmetry of the underlying lattice, many properties related to the lattice structure of the material are automatically included in the model. In this section, we consider the advances in understanding the original, phenomenological formulation of the PFC model, and its application to crystal growth in the diffusion controlled regime.

2.1 Mathematical formulation

Originally the PFC model was phenomenologically postulated in the spirit of the Ginzburg-Landau theory by Elder *et al.* in 2002 [12]. The model consists of an order parameter field that is driven by dissipative, conserved dynamics to minimize a free energy functional, whose ground state exhibits a periodic structure commensurate with the crystal symmetry of interest. More specifically, the deterministic equation of motion for the locally conserved order parameter field $\phi(\mathbf{r})$ in these models is given by

$$\frac{\partial \phi}{\partial t} = M\nabla^2 \frac{\delta F}{\delta \phi}, \tag{2.1}$$

where M is mobility and F is free energy of the system as a functional of the field $\phi(\mathbf{r})$. A minimum requirement for a free energy functional for PFC studies is that

it should have, at least in some parameter range, a ground state exhibiting the periodic structure of interest. The most simple known free energy functional that fulfills this requirement is the form derived by Swift and Hohenberg (SH) for a study of convective instabilities [34]. In such PFC models, sometimes also referred to as SH PFC models, the free energy of the system is given by

$$F\left[\phi(\mathbf{r})\right] = \int d\mathbf{r} \left\{ \frac{\phi(\mathbf{r})}{2} \left[\alpha + \lambda(q_0^2 + \nabla^2)^2\right] \phi(\mathbf{r}) - \frac{h}{3}\phi(\mathbf{r})^3 + \frac{g}{4}\phi(\mathbf{r})^4 \right\}, \tag{2.2}$$

where α, λ, q_0, h and g are phenomenological parameters related to the properties of the material of interest (see e.g. Ref. [13] for discussion of the parameters' relation to elastic constants). Due to its simplicity, Eq. (2.2) is the most common choice of a free energy functional for PFC studies.

For many practical purposes, it is convenient to rewrite Eq. (2.2) by using dimensionless variables. As noted in Ref. [13] for the case when $h = 0$, and as we noted in Publication I for the general $h \neq 0$ case, this can be achieved by introducing a set of new variables,

$$\mathbf{x} = q_0\mathbf{r}; \tag{2.3}$$

$$\psi = \sqrt{\frac{g}{\lambda q_0^4}} \left(\phi - \frac{h}{3g}\right); \tag{2.4}$$

$$\epsilon = \frac{1}{\lambda q_0^4} \left(\frac{h^2}{3g} - \alpha\right). \tag{2.5}$$

All terms that are either constant or linearly proportional to the dimensionless order parameter field ψ can be ignored, as they will not make a contribution to the equation of motion in a conserved model. We then define a dimensionless free energy $\tilde{F}$ as $g\lambda^{-2}q_0^{-5}$ times the original free energy without the constant and linear parts. We then have

$$\tilde{F}\left[\psi(\mathbf{x})\right] = \int d\mathbf{x} \left\{ \frac{\psi(\mathbf{x})}{2} \left[-\epsilon + (1 + \nabla^2)^2\right] \psi(\mathbf{x}) + \frac{1}{4}\psi(\mathbf{x})^4 \right\}. \tag{2.6}$$

Thus, this variable change also shows that the most relevant information contained by the five parameters in Eq. (2.2) can be reduced to two numbers, ϵ and the average

value of ψ. Equation of motion for the field ψ then becomes

$$\frac{\partial \psi}{\partial \tau} = \nabla^2 \left\{ \left[-\epsilon + (1+\nabla^2)^2 \right] \psi + \psi^3 \right\} \tag{2.7}$$

where τ is a rescaled time variable.

2.2 Phase diagram

In order to understand how the free energy defined by Eq. (2.6) gives rise to the desired periodic structures, it is useful to consider *one-mode approximations* to the field ψ. Those are obtained by summing up the Fourier modes corresponding to the first star of the reciprocal lattice of a given lattice structure, and adding a constant to represent the average density of the crystal structure. In the simplest case of one-dimensional striped phase, the one-mode approximation becomes

$$\psi_{stripes}(\mathbf{x}) = \psi_0 + u\left(e^{iqx} + e^{-iqx}\right) = \psi_0 + 2u\cos(qx) \tag{2.8}$$

where ψ_0 is average value of ψ, u is amplitude of the Fourier modes, and q is related to the inverse of the wavelength of density fluctuations. If one substitutes $\psi_{stripes}$ in Eq. (2.6), it is straightforward to evaluate the integrals, and one finds

$$\frac{\tilde{F}_{stripes}}{a_l} = \frac{-\epsilon+1}{2}\psi_0^2 + (-\epsilon + (-q^2+1)^2)u^2 + \frac{1}{4}(\psi_0^4 + 12\psi_0^2 u^2 + 6u^4), \tag{2.9}$$

where $a_l = 2\pi/q$ is the spacing between the stripes. By minimizing Eq. (2.9) with respect to q, one finds that, for any non-zero u, free energy is minimized by $q = 1$. Further, one finds that if $\epsilon - 3\psi_0^2 < 0$, the free energy exhibits a minimum at a non-zero amplitude

$$u = \sqrt{\frac{\epsilon - 3\psi_0^2}{3}}, \tag{2.10}$$

and the free energy at this minimum is found to be

$$\frac{\tilde{F}_{stripes}}{a_l} = \frac{1}{4}\psi_0^4 + \frac{-\epsilon+1}{2}\psi_0^2 - \frac{(\epsilon - 3\psi_0^2)^2}{6}. \tag{2.11}$$

Comparing this with the free energy of a uniform phase,

$$\frac{\tilde{F}_{uniform}}{a_l} = \frac{1}{4}\psi_0^4 + \frac{-\epsilon+1}{2}\psi_0^2, \tag{2.12}$$

obtained from Eq. (2.9) by setting $u = 0$, we find that whenever the non-zero u minimum exists, the periodic phase has a lower free energy than the uniform phase. Therefore in that parameter regime, the periodic phase is energetically favored over the uniform one. Phase diagram of the one-dimensional system in the one-mode approximation would then be obtained by applying the common tangent rule or Maxwell's equal-area construction with the free energies defined by Eqs. (2.9) and (2.12).

As an aside, we note that in addition to providing means for approximate phase diagram calculations, the one mode approximation forms the basis of so-called amplitude expansions. If the amplitude u in Eq. (2.8) (or similar expressions for more complicated phases) is considered a spatially variable field, one can derive approximate equations of motion for the amplitudes from Eq. (2.7) [26, 27, 28, 29, 30, 31]. In the amplitude equation approach, Eq. (2.9) would represent the uniform amplitude limit of a more complicated expression for F as a functional of the amplitude (or, as in many cases, several amplitudes). Such amplitude equations make the PFC model feasible for significantly larger computational domains than accessible through direct numerical integration of Eq. (2.7). However the amplitude equation approximations have their own challenges. In the present work, we will concentrate on challenges related to the PFC models underlying the amplitude equations.

In two dimensions, the one mode analysis also considers an expression similar to Eq. (2.8) for the hexagonal phase. The two dimensional one-mode approximation has been considered in Ref. [13], where also the phase diagram for one and two dimensions is given. It is demonstrated that in the limit where ϵ approaches zero (the limit where the solid-liquid phase transition becomes weakly first order [33]), the results given by the one-mode approximation approach the exact solutions.

In three dimensions, one has to consider the phases exhibiting three dimensional crystal symmetry, in addition to the hexagonal and striped phases. Among the different three dimensional crystal structures, one then finds that in the one-mode approximation, $\tilde{F}$ given by Eq. (2.6) favors the formation of body-centered cubic (BCC) phase over simple cubic, face-centered cubic (FCC) and hexagonal close packed (HCP) structures. The phase diagram obtained for the three dimensional PFC model from the one-mode approximation in the small ϵ limit is shown in Fig. 2.1. In this figure the predictions of the one-mode approximation are also compared to our numerical results presented in Publication I. Numerically the density profiles at each average density were obtained by relaxing the system through numerical integration of Eq. (2.7) using a semi-implicit operator splitting scheme outlined in Appendix A. One-mode approximations were used as initial conditions for different phases.

It is seen in Fig. 2.1 that in the limit of small ϵ, the results obtained from the numerical free energy minimization method and the one mode approximation approach one another. As ϵ increases, the exact coexistence densities obtained from the two methods differ, but qualitatively the one-mode approximation still gives a good description of the phase diagram. For this reason, it was believed that it would only be possible to obtain a stable BCC crystal structure from the SH type PFC models. However, as we extended the numerical analysis to larger ϵ's in Publication I, we found an unexpected result: from $\epsilon = 0.35$ upwards, the stable three-dimensional crystal that forms from the liquid is not BCC, but HCP. Further increasing ϵ we found that beyond $\epsilon = 0.48$ the HCP structure is taken over by the FCC structure. The complete phase diagram obtained from numerical free energy minimization, which is the main result of Publication I, is shown in Fig. 2.2. The importance of the discovery of close packed structures is that it allows the community to study phenomena in the close packed crystal structures, as well as structural phase transitions between the solid phases, using the SH PFC model without making any additional complications to the model. However, work by Wu and Karma

on BCC iron suggests that for accurate modeling of realistic materials, ϵ should be approximately 0.1 [33]. Judging from this criterion, the model may not accurately reproduce all the desired physical properties of the FCC or HCP materials under study. In order to quantitatively study the close packed structures, and also to study some more complicated crystal structures, we believe some modifications to the free energy functional are necessary. Even though some progress in this direction has been reported recently [25, 35, 36], many issues in the problem of quantitatively modeling close-packed structures with the PFC model are still open.

2.3 Application to diffusion controlled crystal growth

In Publication II, we applied the SH PFC model to study the growth of different crystal polymorphs in the regime of diffusion-controlled growth. In a model where diffusive mass transport and the density jump between solid and liquid phases is considered, diffusion controls the rate of a planar solidification front, if the initial liquid has a density that is larger than the crystallization density of the liquid, but smaller than melting density of the solid. In such a situation mass diffusion is the factor limiting the growth process. This is because as time evolves, progressing the front and forming more of the solid (whose density is always at least that of the melting point to be stable) requires transport of mass from further and further away from the interface. Even though the limiting process here is transport of mass, the process is analogous to the more commonly considered case where motion of a planar solidification front is limited by transport of heat away from the interface [37, 38]. In such process one expects the solidification front to propagate as $x \sim \sqrt{\tau}$. Regarding diffusion controlled growth, a question that could only be addressed using an atomistic approach is how the growth rates of stable and metastable crystalline polymorphs and their different facets compare. The PFC model is an ideal model through which these problems can be addressed because in molecular dynamics simulations the diffusion-controlled regime cannot be easily

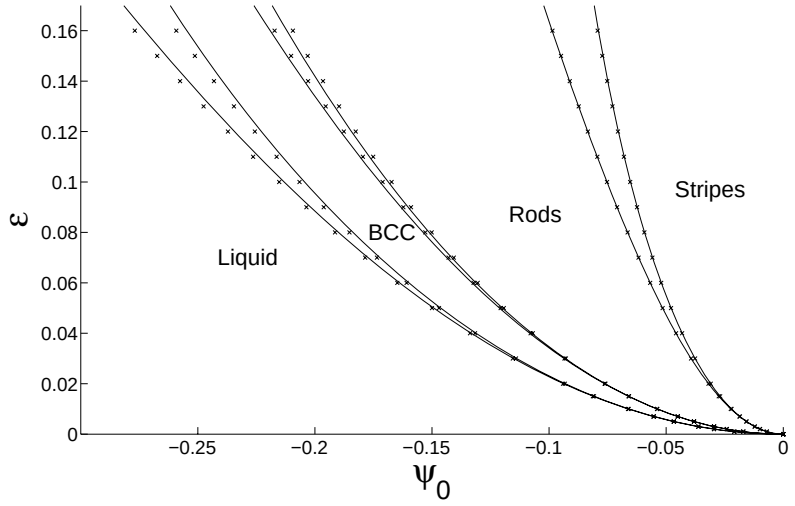

Figure 2.1: Phase diagram of the PFC model in the small ϵ limit. Solid lines represent results from one-mode approximations, and symbols are obtained through numerical free energy minimization. Reprinted from Publication I.

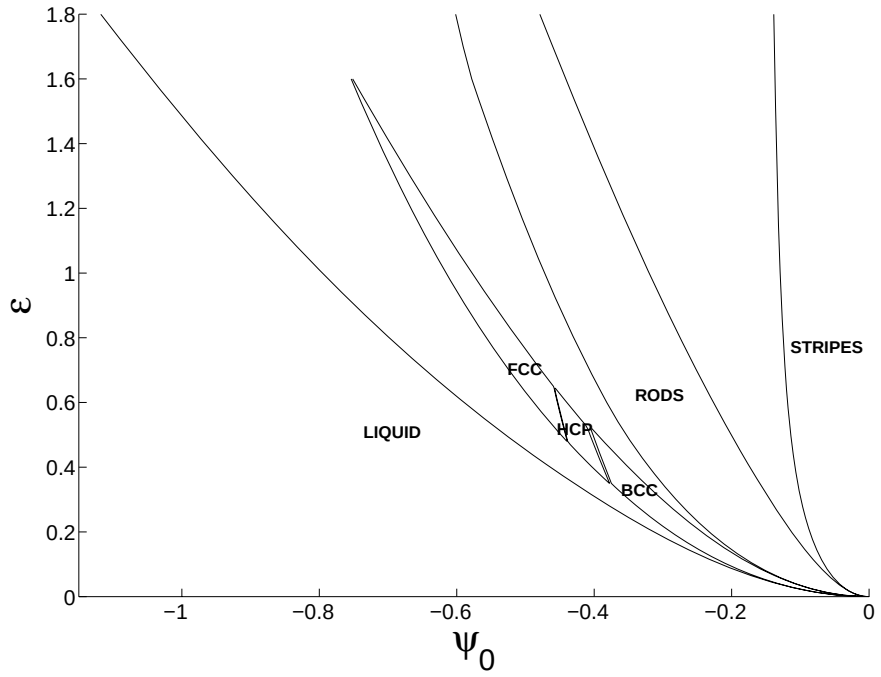

Figure 2.2: Extended phase diagram of the three-dimensional PFC model obtained from numerical free energy minimization. Reprinted from Publication I.

accessed due to computational limitations in time scales accessible by the method.

To carry out this study, we used the model defined by Eqs. (2.1) and (2.2) with parameters that correspond to $\epsilon \approx 0.375$. With these parameters, the stable crystal that forms from the liquid has HCP structure, as can be seen from Fig. 2.2. By observing the free energies as a function of average density carefully, it is seen that all the three phases (BCC, HCP and FCC) are energetically very close, making the parameter choice an ideal one for the study of the effect of crystal structure on the crystallization process.

In order to gain information on the anisotropy of the solid-liquid interfacial free energies, we first determined the equilibrium crystal shapes that minimize free energy for a given cluster volume and crystal structure. For the stable HCP phase, the equilibrium shape also corresponds to global minimum of the free energy, while for the metastable phases, the metastable "equilibrium" shape corresponds to a local minimum of the free energy. The shapes of such crystals reflect the anisotropy of their surface free energy through the well-known Wulff construction. We observed strongly faceted rhombo-dodecahedral, octahedral, and hexagonal-prism shapes for the BCC, FCC, and HCP structures, bound exclusively by the (110), the (111), and the $(10\bar{1}0)$ and (0001) faces. The strong faceting prevented us from accurately defining the anisotropy of the interfacial free energy, except for the case of HCP, where we find $\gamma_{10\bar{1}0}/\gamma_{0001} \approx 1.08$.

For the diffusion controlled growth studies, crystallization was initialized by placing at the center of the simulation box a rectangular slab filled by the one-mode approximation of the density distribution of the bulk crystal. In these studies, we found that after a brief transient the position of the interface as a function of time closely follows the expected $x \sim \sqrt{\tau}$ behavior. Observing the growth process in more detail, we found that density of the liquid in front of the solid varied periodically. This indicates a barrier controlled layerwise growth process, presumably via

2D nucleation consistent with the faceted morphology. This process was also seen to result in relatively large anisotropies in the front velocities. By fitting the resulting interface positions with an equation $x = x_0 + d\sqrt{\tau - \tau_0}$, we were able to compare the velocities of different crystal structures in different crystal directions. For the different facets of BCC, we found a sequence $d_{111} > d_{100} > d_{110}$, and the ratios of coefficients d_{100} and d_{110} were found to agree well with experimental results reported for ^{3}He crystals [39]. For HCP, we found a sequence $d_{11\bar{2}0} > d_{10\bar{1}0} > d_{0001}$, but we were not able to directly compare this result with experiments due to a lack of experimental data in the diffusion-controlled regime. The lack of experimental data also prevented us from comparing the results for FCC phase with experiments. In the case of FCC, we observed $d_{110} > d_{100}$, but we were unable to define d_{111} because the more stable HCP phase grew on top of the (111) face of FCC. In Publication II we also discuss how these results compare with results from molecular dynamics simulations in the interface kinetics controlled regime of growth.

In addition, we investigated how phase selection is influenced by a foreign substrate of simple cubic structure. In these studies, the initial slab placed in middle of the liquid was replaced by a simple cubic structure held in the desired structure by applying an appropriate external pinning potential. The lattice constant, a_0, of the simple cubic substrate was varied in a range that incorporated the interatomic distance of the bulk FCC structure and the lattice constant of the bulk BCC phase. The structure of the crystals that grew in the simulations were found to exhibit a body-centered tetragonal (BCT) structure. The axial ratio c/a (where c and a are the lattice constants of the BCT structure perpendicular and parallel to the surface of the substrate) varied continuously with a_0. At the appropriate values of a_0, the FCC and BCC structures are observed. These results indicate that phase selection of a material grown on top of a substrate can be strongly influenced by the properties of the substrate.

3 Connection between density functional theory and phase field crystal model

Because the order parameter field in the PFC model exhibits periodic variations, it is natural to consider the field as being related to the atomic number density of the underlying system. On the other hand, in studies of classical density functional theory (CDFT), one aims at a microscopic derivation of the static (and more recently dynamic [40]) properties of the systems under study by using the microscopic density as a field variable in the theory. In 2007, Elder *et al.* [32] introduced the assumption of the field under study in the PFC model to be linearly proportional to the atomic number density in CDFT. Under that assumption the PFC model can be viewed as a simplified version of CDFT. In this section, we show some developments to the connection between CDFT and PFC. These include a new variant of the PFC model that is able to reproduce certain properties of the CDFT model with much greater accuracy than the previously presented methods. The quantitative PFC model is applied to study grain boundary energies of body-centered cubic iron.

3.1 Density functional theory of classical systems

Density functional theory of classical systems (CDFT) is essentially a reformulation of classical statistical mechanics, in which the one-particle density is used as a field variable in the theory. Even though the CDFT is less well known than its quantum mechanical counterpart, it is thoroughly discussed in many excellent textbooks involving the theory of classical liquids (see for example Ref. [41] for an elementary introduction to the topic, or Ref. [42] for more advanced discussion), and therefore it will suffice to briefly mention the basic concepts of the theory here.

3.1.1 General formulation

From the grand canonical partition function of an interacting system one can show that the grand potential Ω of the system is a unique functional of the intrinsic chemical potential

$$\mu_{int}(\mathbf{r}) = \mu - u(\mathbf{r}), \tag{3.1}$$

where μ is chemical potential, and $u(\mathbf{r})$ is a spatially varying external field that the system is subjected to. This is a generalization of the usual convention that Ω is a function of temperature, volume and μ to spatially varying external fields. Moreover, it can be shown that

$$\frac{\delta\Omega\left[\mu_{int}(\mathbf{r})\right]}{\delta\mu_{int}(\mathbf{r})} = -\rho(\mathbf{r}), \tag{3.2}$$

where $\rho(\mathbf{r})$ is the ensemble-averaged one-particle density,

$$\rho(\mathbf{r}) = \left\langle \sum_i \delta(\mathbf{r} - \mathbf{r}_i) \right\rangle, \tag{3.3}$$

where the angular brackets indicate an ensemble average, sum over i indicates summation over all particles, and δ is the Dirac delta function. In order to find a functional in which the natural variable is $\rho(\mathbf{r})$ rather than $\mu_{int}(\mathbf{r})$, one performs a functional Legendre transform, which results in the intrinsic free energy,

$$\mathcal{F}\left[\rho(\mathbf{r})\right] = \Omega\left[\mu_{int}(\mathbf{r})\right] - \int d\mathbf{r} \frac{\delta\Omega\left[\mu_{int}(\mathbf{r})\right]}{\delta\mu_{int}(\mathbf{r})}\mu_{int}(\mathbf{r}) = \Omega\left[\mu_{int}(\mathbf{r})\right] + \int d\mathbf{r}\mu_{int}(\mathbf{r})\rho(\mathbf{r}). \tag{3.4}$$

$\mathcal{F}$ can then be shown to be a unique functional of $\rho(\mathbf{r})$ with

$$\frac{\delta\mathcal{F}\left[\rho(\mathbf{r})\right]}{\delta\rho(\mathbf{r})} = \mu_{int}(\mathbf{r}). \tag{3.5}$$

The intrinsic free energy $\mathcal{F}$ is a central quantity in CDFT. Its interpretation, through Eq. (3.5) is such that for any given density field the functional derivative of $\mathcal{F}$ with respect to the density field gives the intrinsic chemical potential that will give rise to the density field of question in equilibrium. In the more usual case, one wants

to study the density field that results from a given μ_{int} (that could correspond, for example, a wall to which a liquid is subjected), which can also be found through Eq. (3.5) by using variational methods. Either way, if $\mathcal{F}$ were known one could determine a unique solution. Unfortunately, in the general case finding $\mathcal{F}$ exactly is a task that is as demanding as calculating the partition function exactly. Therefore, it can be carried out only for a very limited number of systems. One such system is the non-interacting ideal gas, for which it is straightforward to show that

$$\mathcal{F}_{id} = k_B T \int d\mathbf{r} \rho(\mathbf{r}) \left[\ln(\rho(\mathbf{r})\lambda_T^3) - 1 \right], \tag{3.6}$$

where λ_T is thermal de Broglie wavelength. Using this result, it is natural to split the $\mathcal{F}$ of an interacting system into two parts,

$$\mathcal{F} = \mathcal{F}_{id} + \mathcal{F}_{xs}, \tag{3.7}$$

where $\mathcal{F}_{xs}$ is the excess free energy, which is due to interactions between the particles.

Although finding $\mathcal{F}_{xs}$ exactly is for most cases an overwhelmingly challenging task, many feasible approximations to this functional have been proposed in the literature. These approximations include virial expansions, local density approximations [43], methods based on non-locally weighted densities [44, 45], methods based on the geometry of the objects under study [11, 46, 47], etc. Each of these approximations have their own limitations. In what follows, we will briefly discuss perhaps the most simple non-local approximation to $\mathcal{F}_{xs}$ that is feasible to the problem of crystallization, namely the approximation based on a second-order density expansion. For more thorough discussion of the different approximations developed up to date, and the ongoing research in the field, the reader is referred to the textbook by Hansen and McDonald [42] and references therein.

3.1.2 Density expansion

In order to expand $\mathcal{F}_{xs}$ in powers of density, we note that the functional $\mathcal{F}_{xs}$ acts as a generating functional to the family of *direct correlation functions*,

$$\beta \left(\frac{\delta^n \mathcal{F}\left[\rho(\mathbf{r})\right]}{\delta\rho(\mathbf{r}_1)\ldots\delta\rho(\mathbf{r}_n)} \right)_{\rho(\mathbf{r})=\rho_0} = -c^{(n)}(\mathbf{r}_1 \ldots \mathbf{r}_n; \rho_0), \tag{3.8}$$

where $\beta = (k_B T)^{-1}$, $c^{(n)}$ is the n-body direct correlation function, and ρ_0 is the reference density at which the functional derivative is evaluated. Using this with Eqs. (3.1), (3.5), (3.6) and (3.7), it can be shown that if a uniform reference chemical potential $\mu_{int}(\mathbf{r}) = \mu_0$ gives rise to a uniform equilibrium density ρ_0, then

$$-c^{(1)}(\rho_0) = \mu_0 - \ln(\rho_0 \lambda_T^3). \tag{3.9}$$

Using this, we can write the expansion of $\mathcal{F}_{xs}$ up to second order, resulting in the approximate free energy functional,

$$\beta\Delta\mathcal{F}\left[\rho(\mathbf{r})\right] = \int d\mathbf{r}\rho(\mathbf{r})\ln(\rho(\mathbf{r})/\rho_0) - \Delta\rho(\mathbf{r}) - \frac{1}{2}\int\int d\mathbf{r}d\mathbf{r}'\Delta\rho(\mathbf{r})c^{(2)}(|\mathbf{r}-\mathbf{r}'|)\Delta\rho(\mathbf{r}'), \tag{3.10}$$

where Δ denotes the difference with respect to the reference state characterized by ρ_0, and the term proportional to μ_0 has been ignored since it makes no difference in a conserved model. The two-body direct correlation function $c^{(2)}$ that enters Eq. (3.10) is related to the total pair correlation function $h(r)$ of the same system through the Ornstein-Zernike relation,

$$h(r) = c^{(2)}(r) + \int d\mathbf{r}' h(|\mathbf{r}'|)c^{(2)}(|\mathbf{r}-\mathbf{r}'|). \tag{3.11}$$

This also connects $c^{(2)}$ with the structure factor $S(k)$ of the liquid because $S(k)$ is connected to $h(r)$ through

$$S(k) = 1 + \rho_0 \hat{h}(k), \tag{3.12}$$

where $\hat{h}(k)$ is the Fourier transform of $h(r)$. Thus, the function $c^{(2)}$ required for the functional Eq. (3.10) can be obtained through any procedure that is able to provide us with $h(r)$ or $S(k)$ for the system of interest. These include integral equation theories of the structure of liquids, neutron scattering experiments, and molecular dynamics and Monte Carlo computer simulations.

3.1.3 Density functional theory of freezing

In the approach to the study of freezing transition known as CDFT of freezing, one applies CDFT to study the freezing transition. In this approach, the solid is represented by a density field that exhibits the periodic nature of the crystal structure under study. As an explicit example, we may write the density field as

$$\rho(\mathbf{r}) = \rho_0 \left(1 + \Delta\rho^* + \sum_{\mathbf{G}} \mu_{\mathbf{G}} e^{i\mathbf{G}\cdot\mathbf{r}} \right), \tag{3.13}$$

where $\Delta\rho^*$ is the fractional density change in freezing and the Fourier components $\mu_{\mathbf{G}}$ correspond to non-zero reciprocal lattice vectors. This density is then inserted in a free energy functional, such as Eq. (3.10), and the free energy is minimized with respect to the order parameters $\mu_{\mathbf{G}}$ (often the number of parameters is reduced by representing the density as a set of Gaussians centered at the lattice sites). If the free energy is minimized by a set of non-zero $\mu_{\mathbf{G}}$'s, the solid phase is the equilibrium phase. By varying the density ρ_0 around which the expansion is made, one can predict the freezing point of the liquid as well as the density profile of the solid phase that coexists with the liquid.

The approach based on Eqs. (3.10) and (3.13) is essentially the approach that was taken by Ramakrishnan and Yussouff in their pioneering 1979 theory of freezing [10], although their mathematical formulation of the theory was different. Their theory was later rewritten using the present formulation by Haymet and Oxtoby [48]. Nowadays this approach to freezing is known as the second-order theory of freezing. Success of the second-order theory in describing the freezing transition is somewhat surprising since formally the expansion in Eq. (3.10) should be accurate in the limit where $\Delta\rho(\mathbf{r})$ is small. This is not the case in the solid phase. Nevertheless, further studies after Refs. [10] and [48] have shown that even at the second-order level of approximation CDFT is capable of describing a liquid-solid phase transition. The level of agreement of the theory with computer simulations and experiments varies from case to case. For example, for a system of hard spheres, many of the

liquid-FCC transition parameters obtained from the second-order theory are only a few percent off from those obtained from Monte Carlo simulations. In contrast, for a classical one-component plasma, the theory has not been proven capable of describing the transition from a liquid to BCC structure (see Ref. [9] for a more thorough discussion, along with comparison to later versions of CDFT of freezing). The second order theory is therefore a good candidate for connecting the PFC model with microscopical theories of freezing, as far as phase transitions between solid and liquid phases are considered. In order to include a gaseous phase in the PFC model, a more elaborate approximation to $\mathcal{F}_{xs}$ should probably be used as a starting point, but such considerations are beyond the scope of the current work.

3.1.4 Dynamical density functional theory

Until recently, most studies utilizing CDFT have only considered static properties of the systems under study. In 1999, however, Marconi and Tarazona [40] showed that from the equations of motion,

$$\dot{\mathbf{r}}_i = \gamma^{-1}(\mathbf{F}_i + \mathbf{f}_i),\ i = 1 \ldots N, \tag{3.14}$$

where the dot denotes time derivative, γ is a friction coefficient, $\mathbf{F}_i$ is the force from the other particles and an external field acting on particle i, and $\mathbf{f}_i$ is a Gaussian random force that fulfills the fluctuation-dissipation theorem, one can derive an equation of motion for the one-particle density

$$\rho(\mathbf{r}, t) = \sum_i \langle \delta(\mathbf{r} - \mathbf{r}_i(t)) \rangle \,, \tag{3.15}$$

where the angular brackets denote a noise average, instead of the ensemble average involved in the static theories. The derivation proceeds through a coordinate transformation and subsequent noise averaging. In another procedure, Archer and Evans [49] have derived the same equation of motion by using the Smoluchowski equation as their starting point. The equation of motion for $\rho(\mathbf{r}, t)$ resulting from both of

these derivations is

$$\dot{\rho}(\mathbf{r},t) = \gamma^{-1}\nabla \cdot \left(\rho(\mathbf{r},t) \nabla \left(\frac{\delta F\left[\rho(\mathbf{r},t)\right]}{\delta \rho(\mathbf{r},t)} \right) \right), \tag{3.16}$$

where $F\left[\rho(\mathbf{r},t)\right]$ is the Helmholtz free energy of the system described by a density field $\rho(\mathbf{r},t)$ (i.e., intrinsic free energy and the possible contribution from an external field). Such extensions of the CDFT to the study of dynamical phenomena have become known as the dynamical density functional theory of classical systems (DDFT). As noted in the recent work of Ramos *et al.* [23], this equation of motion can also be obtained in the overdamped limit of a more general equation of motion for the number and momentum densities, if the effective Hamiltonian is replaced by the free energy and thermal fluctuations are ignored. Thus, we note that in connection to PFC modeling it would be possible to consider dynamics including momentum conservation. However, in the present work, we have restricted ourselves to consider the dynamics given by Eq. (3.14).

3.2 Derivation of the Swift-Hohenberg phase field crystal model from the density functional theory

3.2.1 Approach of Elder et al. (2007)

Due to the periodic nature of the order parameter field in the PFC model it is not hard to come up with an intuitive interpretation that the field must be related to the atomic number density of the underlying system. Therefore, it is reasonable to assume that the PFC model could be derived from CDFT. The first attempt to establish this connection was presented in 2007 by Elder *et al.* [32] whose derivation we will briefly reproduce in what follows. While Elder *et al.* presented their derivation for both pure materials and binary alloys, we present only the pure material case here, as the current work only considers single component systems.

In Ref. [32], a connection between the functionals given in Eq. (2.2) and Eq. (3.10) was obtained by first defining a dimensionless density deviation n as

$$n(\mathbf{r}) = \frac{\rho(\mathbf{r}) - \bar{\rho}}{\bar{\rho}}, \tag{3.17}$$

where $\bar{\rho}$ is the average value of $\rho(\mathbf{r})$. Substituting this in Eq. (3.10), noting that n averages to zero, and defining $\rho_0 c^{(2)}(\mathbf{r} - \mathbf{r}') = C(\mathbf{r} - \mathbf{r}')$, the free energy change becomes

$$\begin{aligned} \frac{\Delta\mathcal{F}[n(\mathbf{r})]}{k_B T \rho_0} &= V\left[\frac{\bar{\rho}}{\rho_0}\ln\left(\frac{\bar{\rho}}{\rho_0}\right) - \frac{\bar{\rho}-\rho_0}{\rho_0} - \frac{1}{2}\hat{C}(0)\left(\frac{\bar{\rho}-\rho_0}{\rho_0}\right)^2\right] + \\ &\frac{\bar{\rho}}{\rho_0}\left[\int d\mathbf{r}(1+n(\mathbf{r}))\ln(1+n(\mathbf{r})) - \frac{\bar{\rho}}{2\rho_0}\int\int d\mathbf{r}d\mathbf{r}' n(\mathbf{r})C(|\mathbf{r}-\mathbf{r}'|)n(\mathbf{r}')\right], \end{aligned} \tag{3.18}$$

where $\hat{C}(k)$ is the Fourier transform of $C(\mathbf{r} - \mathbf{r}')$. To obtain a functional similar to Eq. (2.2), two approximations to Eq. (3.18) were made in Ref. [32]. First, the local part was expanded as a fourth-order Taylor series,

$$(1+n)\ln(1+n) - n \approx \frac{1}{2}n^2 - \frac{1}{6}n^3 + \frac{1}{12}n^4. \tag{3.19}$$

Then, the non-local part was expanded in terms of gradients by expanding the direct correlation function in k space as

$$\hat{C}(k) \approx \hat{C}(k_m) - E_S\left(\frac{k_m^2 - k^2}{k_m^2}\right)^2, \tag{3.20}$$

where k_m is the point where $\hat{C}(k)$ reaches its maximum value (the main peak), and E_S is a parameter that Elder *et al.* proposed should be fitted such that the expansion reproduces the correct $k = 0$ limit.[1] With the approximations presented in Eqs. (3.19) and (3.20), the free energy functional in Eq. (3.18) becomes

$$\begin{aligned} \frac{\Delta\mathcal{F}[n(\mathbf{r})]}{k_B T \rho_0} &= V\left[\frac{\bar{\rho}}{\rho_0}\ln\left(\frac{\bar{\rho}}{\rho_0}\right) - \frac{\bar{\rho}-\rho_0}{\rho_0} - \frac{1}{2}\hat{C}(0)\left(\frac{\bar{\rho}-\rho_0}{\rho_0}\right)^2\right] + \\ &\frac{\bar{\rho}}{\rho_0}\int d\mathbf{r}\left[\frac{n(\mathbf{r})}{2}\left(1 - \frac{\bar{\rho}\hat{C}(k_m)}{\rho_0} + \frac{\bar{\rho}E_S}{\rho_0}\left(\frac{k_m^2 + \nabla^2}{k_m^2}\right)^2\right)n(\mathbf{r}) - \frac{n(\mathbf{r})^3}{6} + \frac{n(\mathbf{r})^4}{12}\right], \end{aligned} \tag{3.21}$$

[1] Elder *et al.* wrote the expansion as $\hat{C}(k) \approx C_0 + C_2 k^2 + C_4 k^4$. The equivalent form of Eq. (3.20) is used here in order to make connection with latter parts of the text.

where $\hat{C}(0) = \hat{C}(k_m) - E_S$. From Eq. (3.21) it is easy to see that the terms related to n are mathematically similar to Eq. (2.2) with appropriately chosen parameters, establishing a mathematical connection between PFC and CDFT. This connection also provides predictions for how the parameters for the PFC model should be selected.

In Ref. [32], however, no parameters obtained in the presented procedure from the $\hat{C}(k)$ of any realistic system were tested. The first attempt to utilize the fitting procedure presented in Ref. [32] resulted in a large discrepancy between the predicted and the expected material properties, with the crystallization density of three-dimensional copper overestimated by approximately 50 % in the PFC model [50]. In Publication III, this connection was further examined. While the analysis in Ref. [50] was based on the one-mode approximation, we found that, using numerical free energy minimization methods for the case of BCC iron, the essential result remained the same: the point of crystallization was overestimated, this time by about 40 %, and the coexistence gap between solid and liquid phases was found to be only about 0.1 %, where the physical value would be on the order of percents. We also pointed out the inconsistency of expanding $\mathcal{F}_{id}$ and $\mathcal{F}_{xs}$ around different densities. We noted that this inconsistency could be corrected by re-defining n as

$$n(\mathbf{r}) = \frac{\rho(\mathbf{r}) - \rho_0}{\rho_0}, \tag{3.22}$$

and repeating the derivation with $\mathcal{F}_{id}$ expanded in powers of this re-defined n. However, the change led to even further discrepancy between the predictions and the expected results. In this approach, no stable periodic phase could be found at any density.

In Publication III we showed that using the $\hat{C}(k)$ of iron as an input to the second order CDFT of freezing (i.e., Eq. (3.10)), we were able to predict reasonable values for the coexistence densities of solid and liquid phases, and the gap in between. Therefore, we could conclude that the failure of the PFC model to reproduce these

values was related to the approximations made in the derivation of the model presented above and not to the input data. By observing the density profile of the BCC solid predicted by CDFT shown in Fig. 3.1, it became obvious why the approximations made to CDFT had failed. First, the accuracy of the approximation presented in Eq. (3.19) requires that n is a small variable in comparison to unity. As can be observed from Fig. 3.1, n obtained from CDFT reaches values from very close to -1 to as high as several tens. Therefore, the assumption of small n is not justified. Second, accuracy of approximating the non-local part in terms of gradients, as in Eq. (3.20), would require that the field n is slowly varying when compared with the range of $C(r)$. As the range of $C(r)$ is in general the same as the range of the interparticle potential [42], this is quite clearly not the case.

3.2.2 Phase field crystal model of Wu and Karma (2007)

While the procedure to obtain the parameters of Eq. (3.21) presented in Ref. [32] did not lead to accurate results, another procedure for obtaining the PFC model parameters for BCC materials, which provides more accurate predictions, had been presented by Wu and Karma (WK) [33]. In the approach of WK, an amplitude expansion derived from the PFC model was fitted with their Ginzburg-Landau theory for solid-liquid interfaces [51]. In Publication III, we noted that the PFC model of WK could be obtained from the CDFT, if n is defined as in Eq. (3.22) and we allow for two more degrees of freedom, by expanding the logarithmic term as

$$(1+n)\ln(1+n) - n \approx \frac{1}{2}n^2 - \frac{a}{6}n^3 + \frac{b}{12}n^4, \tag{3.23}$$

where we have included the free parameters a and b. The function C is expanded as in the previous approach, but consistent with the work of WK [33], the parameter E_S is chosen such that $\hat{C}''(k_m)$ (where primes denote derivatives with respect to k),

instead of $\hat{C}(0)$, is fitted. With these approximations, the free energy becomes

$$\frac{\Delta\mathcal{F}[n(\mathbf{r})]}{k_B T\rho_0} = \int d\mathbf{r}\left[\frac{n(\mathbf{r})}{2}\left(1-\hat{C}(k_m)+E_S\left(\frac{k_m^2+\nabla^2}{k_m^2}\right)^2\right)n(\mathbf{r})-\frac{a}{6}n(\mathbf{r})^3+\frac{b}{12}n(\mathbf{r})^4\right]. \tag{3.24}$$

The parameters a and b are fitted such that the correct crystallization density and the amplitude of the first mode of density fluctuations in the solid are reproduced in the PFC model. An approximate way to achieve this is through the use of one-mode approximation, i.e., assuming that density of the solid phase is given by

$$n(\mathbf{r}) = 4u\left[\cos(qx)\cos(qy)+\cos(qx)\cos(qz)+\cos(qy)\cos(qz)\right]. \tag{3.25}$$

After substituting this into Eq. (3.24), the parameters a and b are defined s.t. minimum free energy of the solid equals that of the liquid, ensuring existence of a stable solid phase. Additional constraint is provided by requiring that the amplitude u that minimizes free energy of the solid equals a fitted value u_s, which is obtained from e.g. molecular dynamics simulations. The resulting relations for a and b are

$$a = \frac{3}{2S(k_m)u_s}; \qquad b = \frac{4}{30S(k_m)u_s^2}, \tag{3.26}$$

where $S(k_m) = (1-C(k_m))^{-1}$ through the Ornstein-Zernike relation. With $S(k_m)^{-1} = 0.332$ and $u_s = 0.72$, as obtained through MD simulations of iron by WK [33, 51], these relations give $a = 0.6917$ and $b = 0.08540$. The parameter b is particularly different from unity, i.e., the value obtained by the procedure of Ref. [32]. With these parameters and the free energy given by Eq. (3.24), we were able to reproduce the results of Wu and Karma [33], namely that there exists a solid phase at a reasonable density and the free energy of solid-liquid interfaces obtained from the model are in very good agreement with results obtained from molecular dynamics simulations. However, we also found that the bulk moduli of the solid and liquid phases were now underestimated by the model for the reason of a drastic underestimation of $|\hat{C}(0)|$. For the same reason, we found that the gap between coexistence densities of solid and liquid phases was too large by almost an order of magnitude. We found no method to correct for the discrepancy of $|\hat{C}(0)|$ within the framework

of the Swift-Hohenberg PFC model without compromising the value of $\hat{C}''(k_m)$ that affects both surface and elastic properties. Therefore, we sought a generalization of the model, which will be discussed in the next section.

3.3 Eighth-order phase field crystal model

3.3.1 Local formulation

The eighth-order fitting (EOF) version of the PFC model, presented in Publication III, was born out of the conclusion that all means of obtaining the parameters of the Swift-Hohenberg (SH) PFC from the CDFT resulted in a compromise between the surface/elastic and bulk properties of the material under study. From those studies, we could, however, speculate that if we were able to fit the correct $\hat{C}(0)$, k_m, $\hat{C}(k_m)$ and $\hat{C}''(k_m)$ in the model, we would probably be able to produce a more realistic model. Using the expansion presented in Eq. (3.20), it was not possible to fit the four desired properties, because the expansion only includes three parameters. For that reason, another parameter was included in the model by expanding $\hat{C}(k)$ as

$$\hat{C}(k) \approx \hat{C}(k_m) - E_S \left(\frac{k_m^2 - k^2}{k_m^2} \right)^2 - E_B \left(\frac{k_m^2 - k^2}{k_m^2} \right)^4 , \tag{3.27}$$

where the parameter E_S is fitted to give the correct $\hat{C}''(k_m)$ and E_B is fitted with $\hat{C}(0)$. An example of this function for the case of iron is shown in Fig. 3.2 along with comparison to the original $C(k)$ and the two different possibilities to fitting with Eq. (3.20). It can be seen that the eighth-order expansion matches the original $\hat{C}(k)$ fairly well from the $k = 0$ limit up to the first peak.

Apart from using Eq. (3.27) instead of Eq. (3.20), the EOF method as presented in Publication III is identical to the fitting procedure adapted for the SH PFC model from the work of Wu and Karma [33] (that we will hereafter refer to as the fourth-order fit, FOF). That is, the local term is expanded as in Eq. (3.23) with a and b

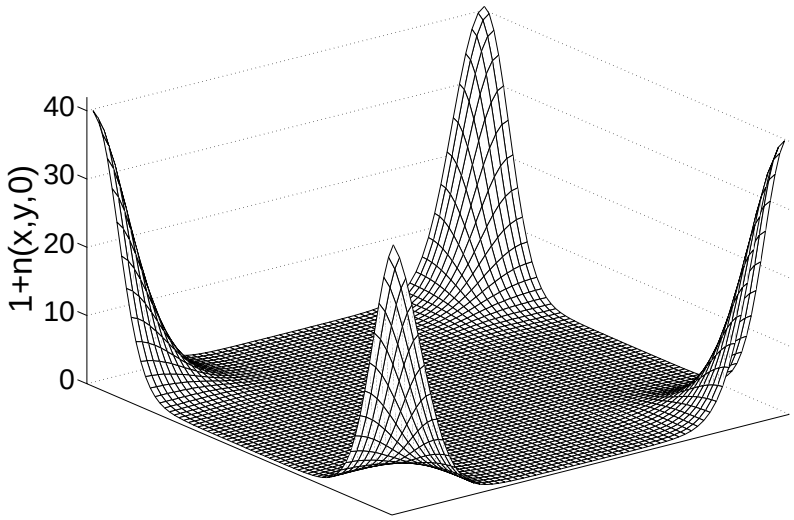

Figure 3.1: Local density in the (100) plane of BCC iron coexisting with its melt, as predicted by the second-order CDFT of freezing. Reprinted from Publication III.

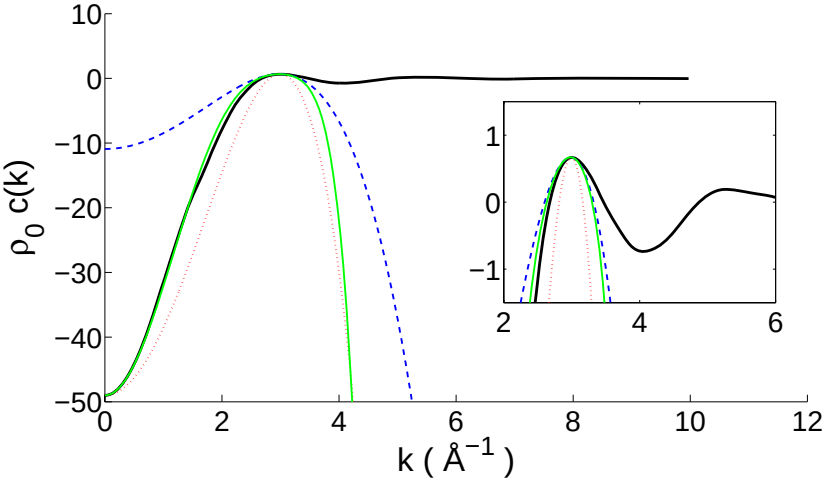

Figure 3.2: Direct correlation function $\hat{C}(k)$ of liquid iron (black line) and the expansions used in different PFC models in Publication III: green solid line is the fit used in the EOF, blue dashed line is from the FOF and red dotted line is the three-parameter fit to C_0 and the first maximum.

chosen through Eq. (3.26). The free energy of the EOF model then becomes

$$\frac{\Delta\mathcal{F}[n(\mathbf{r})]}{k_BT\rho_0} = \int d\mathbf{r}\left[\frac{n(\mathbf{r})}{2}\left(1-\hat{C}(k_m)+E_S\left(\frac{k_m^2+\nabla^2}{k_m^2}\right)^2+E_B\left(\frac{k_m^2+\nabla^2}{k_m^2}\right)^4\right)n(\mathbf{r}) - \frac{a}{6}n(\mathbf{r})^3+\frac{b}{12}n(\mathbf{r})^4\right]. \tag{3.28}$$

Even though the addition of a term including gradients up to eighth order is a relatively small modification of the model, we were able to demonstrate that it results in significant improvements in some thermodynamic properties of the model. With this modification, the predictions for bulk moduli of solid and liquid phases, as well volume change in freezing, were very reasonable in comparison to molecular dynamics simulations and experiments, while the predictions for surface free energies were as good as those obtained from FOF PFC. Comparisons of different model results and experiments are summarized in Table 3.1.

The good agreement between CDFT and EOF may seem surprising, given the discrepancies in the derivation pointed out earlier. The agreement for the bulk properties may seem even more surprising, if one notices how drastically different density profiles the models predict for the solid phase. Prediction from EOF is shown in Fig. 3.3, while that from CDFT is found in Fig. 3.1. The relatively sharp, Gaussian-like peaks obtained from CDFT are smeared out to a density profile almost equal to the one-mode approximation, Eq. (3.25). This results from the expansion in Eq. (3.27), which places a high free energy penalty for the Fourier modes corresponding to wave vectors $k > k_m$. Excluding the modes corresponding to shorter wavelengths is a desirable property of the model from a numerical perspective, as it eases the requirement for the grid spacing in any numerical implementation of the model. From the results presented in Table 3.1, it seems that much of the error induced by this truncation of the higher harmonics in the bulk properties can be overcome through appropriate choice of the parameters a and b.

Table 3.1: Comparison of physical quantities of iron in different models with experiments and molecular dynamics simulations from Publication III.

Quantity	**Expt.**/MD	CDFT	FOF PFC	EOF PFC
Expansion in melting (Å^3/atom)	**0.38** [52]	0.29	2.07	0.43
Solid bulk modulus (GPa)	**105** [53] [a]	101.7	22.2	94.5
Liquid bulk modulus (GPa)	**96.2** [54]	98.0	18.6	93.2
Surface Energy (100) (ergs/cm^2)	177.0 [33]	91.9	207.1	165.7
Surface Energy (110) (ergs/cm^2)	173.5 [33]	89.2	201.7	161.5
Surface Energy (111) (ergs/cm^2)	173.4 [33]	86.9	194.8	157.2
anisotropy ϵ_4 (%)	1.0 [33]	1.5	1.3	1.3

[a] Linear extrapolation from lower temperatures.

3.3.2 Application to grain boundaries of body-centered-cubic iron

Encouraged by the EOF PFC model's success in predicting surface and bulk properties of iron in Publication III, we studied the symmetrically tilted grain boundaries of iron using the same model in Publication IV. Three choices of tilting axes, $\langle 100 \rangle$, $\langle 110 \rangle$ and $\langle 111 \rangle$, were studied. The calculations were performed at a density $1.030\rho_0$, which is close to the melting point of the solid. In order to carry out these calculations, a computational box of dimensions (L_x, L_y, L_z), and periodic boundary conditions in all directions were used. The box was initialized by the one-mode approximation, Eq. (3.25), first rotated such that the rotation axis is perpendicular to the z direction. Then in the region $x = 0 \ldots L_x/2$, the one-mode approximation was rotated in the (x, y) plane by an angle $-\theta/2$, and in the region $x = L_x/2 \ldots L_x$ by an angle $\theta/2$, creating two symmetrically tilted grain boundaries located at $x = 0$ and $x = L_x/2$ with a tilting angle θ. Then the system was equilibrated using conserved dynamics with a semi-implicit operator splitting scheme [55] outlined in Appendix A. Grain boundary energies (GBEs) were obtained from the final configurations by

calculating the free energy excess per grain boundary area.

Three example final configurations for the $\langle 100 \rangle$ case are shown in Fig. 3.4. GBEs as a function of tilting angle θ for all three choices of tilting axis are shown in Fig. 3.5. In the low angle limit of these figures, we observe roughly linear dependence of GBE on θ due to constant build-up of dislocations at the boundary. This behavior is consistent with the theory of Read and Shockley [56]. At large angles, the dependence of GBE on θ is generally weaker. However, several local minima, some stronger and some weaker, are observed. Most of these local minima correspond to angles of relatively small coincidence lattice (CSL) Σ. The most pronounced local minimum observed in Fig. 3.5 corresponds to BCC(112) $\langle 110 \rangle$ $\Sigma 3$ (tilt axis $\langle 110 \rangle$ and $\theta = 109.47°$) grain boundary, which is a twin boundary.

Comparing our results with results obtained using molecular dynamics method with Finnis-Sinclair potential by Shibuta *et al.* [57], we find generally good qualitative agreement. Most, although not all, local minima are found at the same misorientation angles. In addition, our ratios of the local minimum GBEs at BCC(112) $\langle 110 \rangle$ $\Sigma 3$ and BCC(121) $\langle 111 \rangle$ $\Sigma 3$ (tilt axis $\langle 111 \rangle$ and $\theta = 60°$) to the maximum GBE agree well with the results of Shibuta *et al.* [57]. In another atomistic approach to the subject Zhang *et al.* [58] found, using molecular statics with modified analytical embedded atom method, a strong correlation between CSL Σ and GBE in BCC iron. Even though we found that most of the local minima we observed do correspond to small CSL Σ boundaries, we also observed small CSL Σ boundaries that are not local minima of GBE. Therefore, our results presented in Publication IV generally agree with those of Shibuta *et al.* [57], but not fully with those of Zhang *et al* [58]. A possible explanation for this is that our calculations, as well as those of Ref. [57] were performed at an elevated temperature, while Ref. [58] assumes absolute zero temperature.

Experimentally, the large angle grain boundary energy of δ iron has been deter-

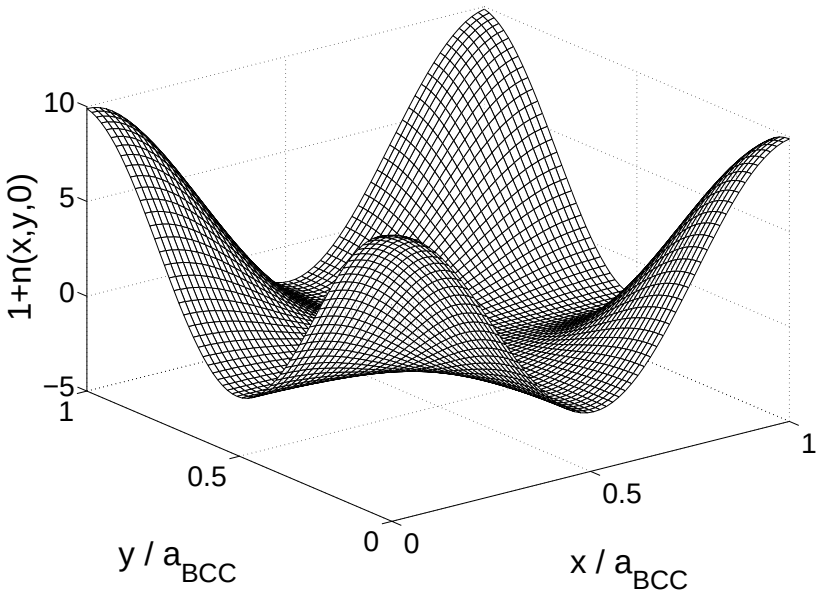

Figure 3.3: Local density n in (100) crystal planes of BCC solid coexisting with liquid in the EOF PFC model. From Publication III.

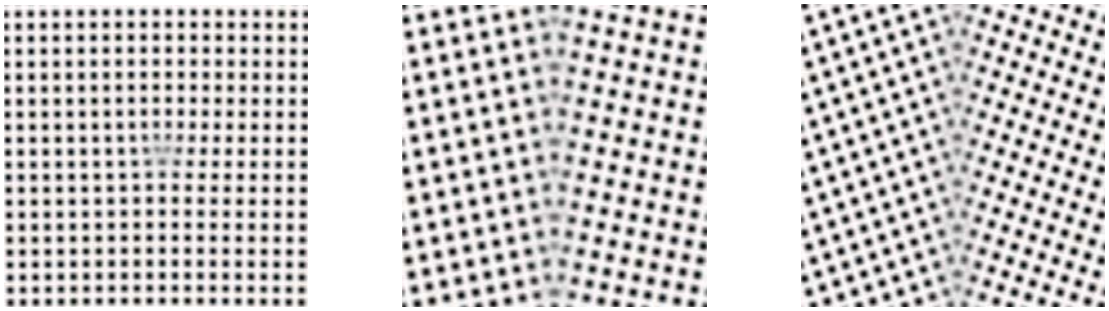

Figure 3.4: Example final configurations from the $\langle 100 \rangle$ case. The gray scale in these figures corresponds to $n(x, y, 0)$. On the left, we show the low-angle bcc(0 64 1) $\langle 100 \rangle$ $\Sigma 40975$ ($\theta = 1.79°$) boundary, where one clearly sees a single dislocation. The middle figure shows a large angle bcc(051) $\langle 100 \rangle$ $\Sigma 13$ ($\theta = 22.62°$) boundary, and the figure on the right shows the bcc(031) $\langle 100 \rangle$ $\Sigma 5$ ($\theta = 36.87°$). From Publication IV.

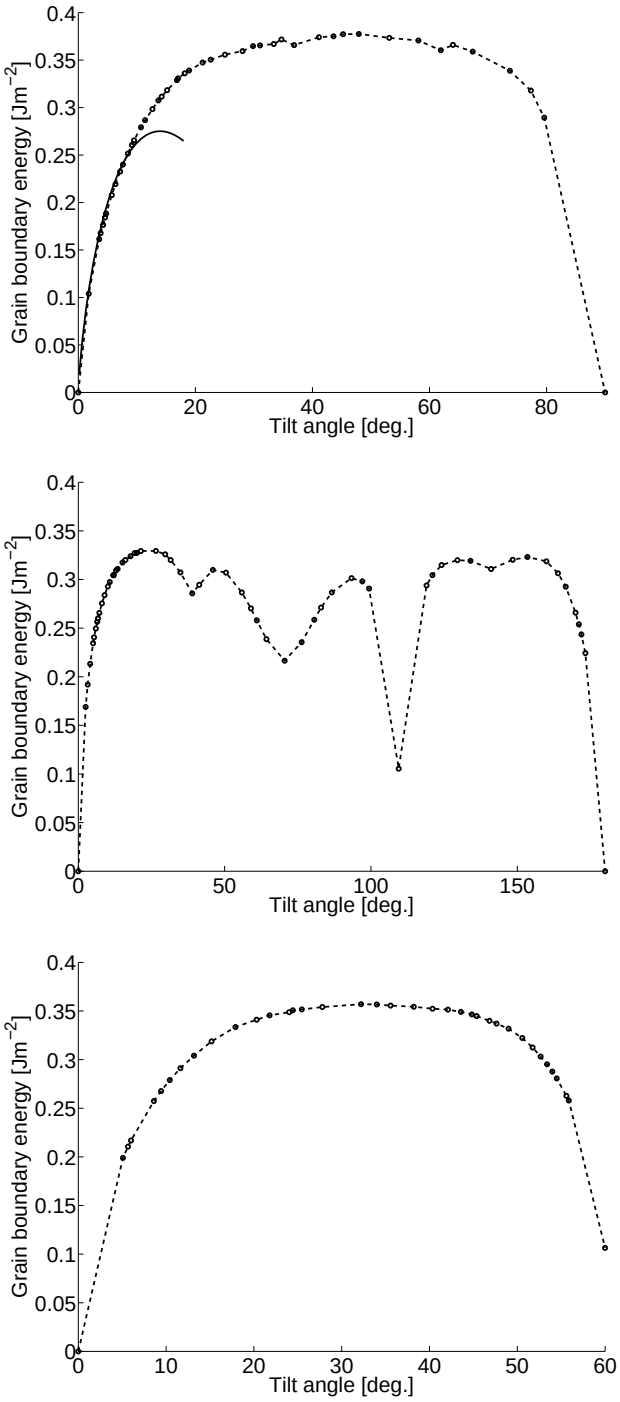

Figure 3.5: Grain boundary free energy as a function of the misorientation angle θ when the tilt axis is in the $\langle 100 \rangle$ (top), $\langle 110 \rangle$ (middle) and $\langle 111 \rangle$ (bottom) direction. For the $\langle 100 \rangle$ case solid line shows the best fit to the Read-Shockley equation at small tilt angles and dashed lines are guides to the eye. From Publication IV.

mined to be 0.468 Jm^{-2} [59], in relatively good agreement with our maximum value of 0.377 Jm^{-2}. The other above-mentioned atomistic studies of GBEs in iron overshoot the experimental value by a large margin, probably in part due to the smaller temperatures involved, and partly because the quantity they measure from simulations is excess energy associated with the grain boundary, whereas in experiments and in PFC, it is the excess free energy of the boundary that is measured. It is also worthwhile noting that the agreement of our results with experimental values from Ref. [59] for the ratio of large angle grain boundary energy to the solid-liquid surface free energy is even better: $E_{gb}/\sigma_{s-l} \approx 2.16$ in the present model (solid-liquid surface energy from Publication III), where the values from Ref. [59] give $E_{gb}/\sigma_{s-l} \approx 2.29$.

Summarizing the results of Publication IV, the EOF PFC model seems very capable of describing grain boundaries in BCC iron, showing the potential of EOF in quantitative modeling of phenomena where grain boundaries play an important role.

3.3.3 Non-local formulation

Despite the quantitative success of the EOF model in Publications III and IV, the weak points about derivation of the model, mentioned previously in the context of the derivation of Elder *et al.* [32], are still valid. Specifically the approximations made in deriving the model still assume that the field n is both small and slowly varying. In addition, comparing the n fields resulting from CDFT and EOF (Figs. 3.1 and 3.3) it is clear that the solution of the EOF model is not an accurate approximation to the actual density field. Most prominently, in EOF the field reaches values that are below -1 corresponding to negative densities. Therefore, it remained questionable whether we could claim that the EOF model was firmly based on first principles.

In Publication III, we argued that the correct interpretation of the field n would

probably be obtained by applying a Fourier filter on the original density field. In Publication V, we showed how this intuitive idea can be used to reformulate the derivation of the model in a new framework. In this derivation, instead of insisting that the field n in the EOF model is locally and linearly related to ρ through Eq. (3.22), we assume they are related through a weighting function w as

$$n(\mathbf{r}) = \rho_0^{-1} \int d\mathbf{r}' w(|\mathbf{r} - \mathbf{r}'|)(\rho(\mathbf{r}) - \rho_0), \tag{3.29}$$

where w is chosen such that its Fourier transform is given by

$$\hat{w}(k) = \sqrt{\frac{1 - \hat{C}(k)}{1 - \hat{C}_{EOF}(k)}}. \tag{3.30}$$

Here, $C_{EOF}(k)$ is the "approximation" to $C(k)$ given by Eq. (3.27). The function $\hat{C}_{EOF}(k)$ follows the original $\hat{C}(k)$ very closely from the $k = 0$ limit up to the main peak at k_m. Beyond this point, the two curves separate, with $\hat{C}(k)$ approaching zero in an oscillatory fashion while $\hat{C}_{EOF}(k)$ approaches the negative infinity, so that $\hat{w}(k)$ will fall close to zero after the main peak. Therefore the field n would closely resemble the observed solutions of the EOF model, even if ρ used as input in Eq. (3.29) were highly peaked as in CDFT.

With this definition of n, we were able to show that the linear part of the free energy of CDFT (linearization of Eq. (3.10)) can be exactly written as

$$\begin{aligned} \frac{\beta \mathcal{F}_{lin}}{\rho_0} &= \frac{\rho_0^{-2}}{2} \int\int d\mathbf{r} d\mathbf{r}' \, \Delta\rho(\mathbf{r}) \left(\delta(\mathbf{r} - \mathbf{r}') - C(\mathbf{r} - \mathbf{r}')\right) \Delta\rho(\mathbf{r}') \\ &= \frac{1}{2} \int d\mathbf{r} n(\mathbf{r}) \left(1 - \hat{C}(k_m) + E_S \left(\frac{k_m^2 + \nabla^2}{k_m^2}\right)^2 + E_B \left(\frac{k_m^2 + \nabla^2}{k_m^2}\right)^4\right) n(\mathbf{r}), \end{aligned} \tag{3.31}$$

where δ is the Dirac delta function. While the linear part of the free energy of EOF arises trivially in this approach, it is not as easy to derive a practically applicable form for the non-linear parts of the free energy. This is because the non-local definition of n makes the non-linear terms, which are local in ρ, non-local in n. In Publication V we argue that $\mathcal{F}_{lin}$ defined by Eq. (3.31) already provides a preferred wavelength of density fluctuations in the system and a large free energy penalty for

Fourier modes with $k \gg k_m$ (that in this formulation is a desired property of the model instead of a result of a questionable approximation). Therefore the use of a functional that is local in terms of the field n may be justified, if the amplitudes of the density fluctuations vary on length scales larger than the range of the weighting function. The simplest possible such functional is

$$\frac{\beta\mathcal{F}_{nl}}{\rho_0} = \int d\mathbf{r} \left(-\frac{a}{6} n(\mathbf{r})^3 + \frac{b}{12} n(\mathbf{r})^4 \right). \tag{3.32}$$

With this admittedly somewhat *ad hoc* choice of $\mathcal{F}_{nl}$, Eqs. (3.31) and (3.32) add up to the previously defined EOF free energy, Eq. (3.28), although the underlying approximations are very different. One crucial difference in these two derivations, in addition to the different approximations involved, is that the current derivation does not suggest that $a = b = 1$, in contrast to the previous version based on Taylor expansion. By approximating the underlying density field ρ by a set of normalized Gaussian peaks in a perfect triangular lattice, we argue in Publication V that this procedure suggests that the parameters should be approximately $a = 3/4$ and $b = 1/5$. However, this choice is somewhat subjective and therefore we believe it is best to use numerical methods to optimize the parameters in such a way that the desired freezing point of the liquid and amplitude u of the solid phase are reproduced in the model. The parameters we obtain through such a scheme are, however, much closer to $a = 3/4$ and $b = 1/5$ than $a = b = 1$. Thus the Gaussian approximation is a better justification to the model than the simple Taylor expansion.

Dynamical equation of the EOF model, which is given by

$$\begin{aligned} \frac{\partial n}{\partial \tau} &= \nabla^2 \left(\frac{\delta F_{EOF}}{\delta n} \right) \\ &= \nabla^2 \left[\left(1 - \hat{C}(k_m) + E_S \left(\frac{k_m^2 + \nabla^2}{k_m^2} \right)^2 + E_B \left(\frac{k_m^2 + \nabla^2}{k_m^2} \right)^4 \right) n - \frac{a}{2} n^2 + \frac{b}{3} n^3 \right], \end{aligned} \tag{3.33}$$

was justified by choosing the simplest possible model satisfying the requirements for conserving the total mass and evolving towards minimum of the free energy. We note that this approaches the same dynamics as DDFT in the near-uniformity limit for the Fourier modes up to k_m (linearized version of Eq. (3.16) is $\partial_\tau \hat{n}(k) =$

$-k^2(1-\hat{C}(k))\hat{n}(k)$ while that of Eq. (3.33) would be similar with $\hat{C}$ replaced by $\hat{C}_{EOF}$). Far from uniformity in the solid phase, Eq. (3.33) probably results in faster diffusion of matter than the DDFT model from which it is derived. However, for studying isothermal solidification of a single component system, we believe that the diffusion rate and attachment kinetics on the liquid side of a moving solidification front are the dominant factors determining the rate of growth.

3.3.4 Comparison to dynamical density functional theory

In Publication V, we compare the predictions of the EOF model to predictions of second-order CDFT, as well as two fourth-order PFC models. The system under study is a two-dimensional array of Brownian particles interacting via an inverse twelfth-power pair potential, evolving in time through overdamped dynamics. For this system, we compare predictions from different models for both static properties of the solid and liquid phases, as well as rates of crystal front propagation.

As the DDFT model in this study, we used a second-order expansion of the free energy, Eq. (3.10), along with the equation of motion, Eq. (3.16). The function $\hat{C}(k)$ was found by using the Ornstein-Zernike equation, Eq. (3.11), with the closure relation of Percus and Yevick [60]. Freezing point of the liquid was identified as the point where grand potentials of solid and liquid phases were equal, and the $\hat{C}(k)$ computed at that density was used as an input for the remainder of the calculations.

Results of DDFT were compared to similar predictions from EOF after appropriate fitting of the parameters a and b. In addition, the results were compared with the fourth-order PFC approach adopted from Wu and Karma [33], i.e. the FOF, and with "PFC1" model derived from the DDFT in Ref. [17]. Free energy of the PFC1 model is Eq. (3.10), with the function $\hat{C}(k)$ replaced by the form used in the FOF, and the excess part $\mathcal{F}_{xs}$ then multiplied by an appropriate constant to adjust the

freezing point. The dynamical equation of the PFC1 model is Eq. (3.16), with the appropriate free energy.

For the static properties, we found that the freezing density obtained from CDFT is larger than that obtained from atomistic simulations [61] by approximately 7 %. The width of the coexistence gap is well reproduced: where molecular dynamics simulations imply $\Delta\rho^* = (\rho_s - \rho_l)/\rho_l \approx 2\%$ [61] (ρ_s and ρ_l are densities of solid and liquid phases at coexistence), our CDFT result is $\Delta\rho^* = 2.20\%$. The EOF model is able to reproduce this result with satisfactory precision giving $\Delta\rho^* = 1.57\%$, while the fourth-order PFC models result in larger errors in opposite directions: $\Delta\rho^* = 7.70\%$ in FOF and $\Delta\rho^* = 0.68\%$ in PFC1. For interfacial free energies, we find that EOF and FOF give a good representation of both the interface thickness and the free energy in comparison to CDFT. PFC1 results in an interface layer that is significantly wider than in all the other models, and interfacial free energy that is more than an order of magnitude smaller than in the other models.

The solidification front dynamics in the DDFT and PFC models were studied by growing a hexagonal crystal from an undercooled liquid (i.e., a liquid with an initial density $\rho_i > \rho_l$) in the [10] direction. In the direction perpendicular to the solidification front propagation, the size of the array in our computations is exactly one interparticle spacing and periodic boundary conditions are used. Due to the periodic boundaries our simulations represent an infinitely wide crystal seed that propagates into the liquid. Initial condition was such that several monolayers of perfect solid are placed in the middle of the undercooled liquid at density ρ_i, with a slight smoothing in the boundary of solid and liquid phases. Once the simulation starts, the solid seed grows in both directions and we measure its position as a function of time.

If the undercooling is small such that $\rho_i < \rho_s$, then formation velocity of the solid (whose density is always at least ρ_s to be stable) is limited by the diffusion of mass to the interface in a manner analogous to the more commonly considered case where

growth of the solid is limited by transport of heat away from the solidification front [37]. As the solidification front propagates, the layer through which diffusion must take place widens and one expects the solidification front to propagate as $x \sim \tau^{0.5}$. Such diffusion-controlled growth was also studied for the different three dimensional crystal polymorphs in Publication II. In Publication V, we also considered cases when density of the liquid from which the solid is formed exceeds ρ_s, such that propagation of the solidification front does not require diffusion of additional mass to the interface. In this regime, one expects the front to propagate with a constant velocity (i.e. $x \sim t$) that depends on the attachment rate of particles on the surface.

In the regime $\Delta = (\rho_i - \rho_l)/(\rho_s - \rho_l) < 1$ where diffusion controlled growth is expected, we have fitted a function

$$x = x_0 + d(\tau - \tau_0)^{\frac{1}{2}} \tag{3.34}$$

in the surface positions as a function of time. The results of these fits are shown in Fig. 3.6. The data are only shown for undercoolings up to $\Delta = 0.6$ because beyond this value we have less confidence in having reached a steady state growth because of finite-size effects. Due to scaling properties of the problem, one expects the position of the interface to depend on the dimensionless undercooling Δ and $\sqrt{D\tau}$, where $D = 1 - \hat{C}(0)$ is the effective diffusion constant in a given model.[2] We illustrate this in the inset of Fig. 3.6, where we show that the d scaled by $\sqrt{D}$ as a function of Δ in all the studied models closely follow the same curve. This indicates that differences in microscopic details of these models are unimportant in determining the solidification front velocity in the diffusion controlled regime. These scaling properties of the problem are the reason why EOF, which has exactly the same D and close to the same $\Delta\rho^*$ as DDFT, reproduces the result of DDFT so much more accurately than FOF, which results in a d that is approximately an eighth of the value obtained from DDFT for the same ρ_i. The scaling argument also suggests that the close agreement of PFC1 to EOF and DDFT in the small density limit probably

[2]With this definition we note that in the limit of small, long-wavelength density fluctuations, all the models studied reduce to the diffusion equation $\partial_\tau n = D\nabla^2 n$

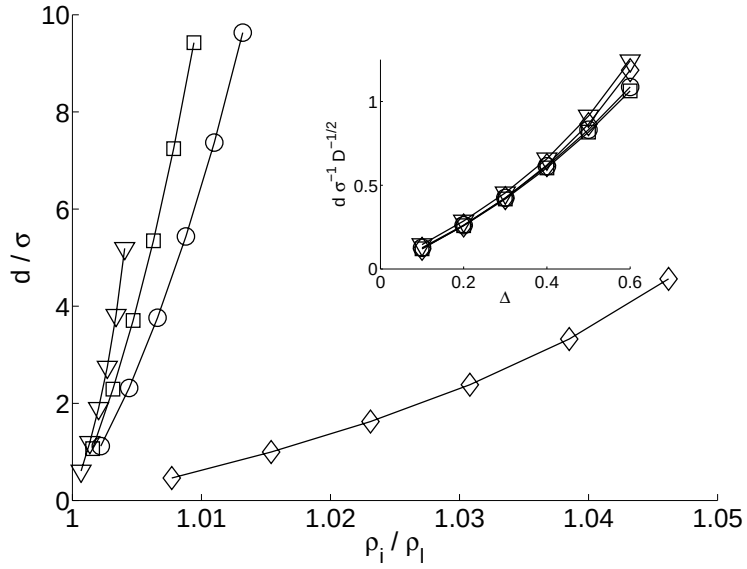

Figure 3.6: Growth rates d obtained in the diffusion controlled regime. Circles are results from the DDFT model, squares from EOF, diamonds from FOF and triangles from PFC1, with lines connecting the symbols. Inset shows scaled data with $\Delta = (\rho_i - \rho_l)/(\rho_s - \rho_l)$.

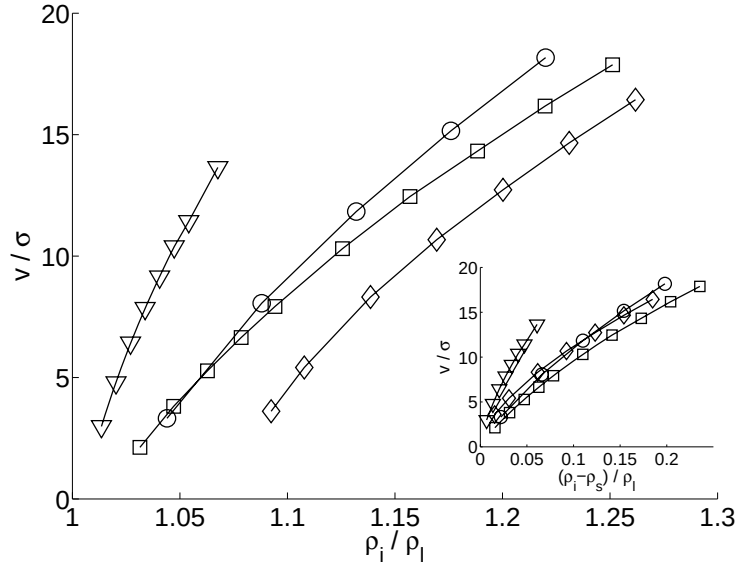

Figure 3.7: Growth velocities v obtained in the kinetics controlled regime. Symbols as in Fig. 3.6.

results from a cancelation of errors due to smaller D and smaller $\Delta\rho^*$ in the PFC1 model.

In the regime $\Delta > 1$ we fitted the results to the expected linear growth law,

$$x = x_0 + v\tau. \tag{3.35}$$

The resulting v as a function of ρ_i from all the models are shown in Fig. 3.7. As expected, the front velocity increases as the initial density is increased in all the models. It is also apparent that, for any given initial density, the velocity obtained from EOF is the closest approximation to DDFT among the PFC models tested here. If the density axis is rescaled by substracting the density of the solid coexisting with the liquid, the results from FOF seem to agree with DDFT practically as well as those from EOF, as shown in the inset of Fig. 3.7. On the other hand, the velocities observed in the PFC1 model seem to be significantly overestimated when compared with the results from all the other models studied even after rescaling the densities. In summary, from the comparison of the EOF model to the DDFT, FOF and PFC1 models, we are able to conclude that the EOF model gives the closest approximation to DDFT among the PFC models studied, for both static and dynamic properties.

4 Summary

The Phase field crystal (PFC) model, introduced less than a decade ago, is a novel approach to modeling phenomena involving atomistic length and diffusive time scales. Although the method has already proven itself useful in modeling various phenomena, important questions about the model remain unsolved from both theoretical and practical perspectives. In the present thesis, we have addressed several challenges related to the PFC model and applied the model to study grain boundaries and crystallization.

We have calculated an extended phase diagram for the simplest and most widely used variant of the PFC models in three dimensions. The calculation of the phase diagram by numerical methods revealed that the model is able to produce stable close-packed crystal structures, in addition to the body-centered cubic structure, which was previously known to exist as a stable phase in the model. The importance of the discovery of stable close-packed structures is that it allows the community to study phenomena in such structures using PFC without making any additional complications to the model. The simple PFC model was also applied to study anisotropy of diffusion-controlled growth in different crystal polymorphs, a problem that has been unattainable for other modeling methods where the atomistic length scale is explicitly present. Our results indicate a barrier-controlled layerwise growth process, presumably via 2D nucleation, and the anisotropy of growth in the simulations seems to be in fair agreement with experiments in cases where experimental data is available.

We have also examined the connection that can be made between the PFC model and classical density functional theory (CDFT). By examining how this connection was established by others, we were able to demonstrate the strengths and weaknesses of their approaches. Based on these considerations, we proposed our own

version of the PFC model, which we call the eighth-order-fitting (EOF) PFC model. First, the EOF model was shown to reproduce certain physical properties of iron with significantly higher precision than the previously presented methods, without making the model numerically more demanding to any significant extent. The EOF model was then applied to study grain boundaries of body-centered cubic iron near its melting point, and the resulting grain boundary energies were in good agreement with experiments and molecular dynamics simulations. Then, after reformulating the EOF model in terms of a weighted density, its predictions for growth rates of two dimensional crystal were compared against a dynamical extension of CDFT, as well as other PFC models. The results indicate that, among the PFC models studied, EOF gives the most accurate approximation to CDFT for both static and dynamic properties.

To summarize, we believe the studies presented in this thesis have advanced the methodology of PFC modeling from both practical and theoretical perspectives: on one hand, by opening new possibilities in modeling different materials and, on the other, by basing the model more firmly on statistical mechanical CDFT. Despite these advances, there still remain plenty of unresolved issues concerning the PFC model. One topical challenge that was briefly touched upon in the context of the phase diagram is quantitative modeling of close-packed crystal structures with PFC. Although in three dimensions the EOF model is able to describe body-centered cubic materials with quantitative precision, our unpublished calculations suggest that it could not be applied to modeling close-packed phases without modifications to the free energy functional. Although phenomenological models that fit the purpose of modeling close-packed structures do exist, we believe there would be demand for an EOF-like quantitative approach to modeling such structures. Another important problem is the modeling of mixtures of different elements. Most materials we observe in reality are in fact mixtures of many different species. Therefore, being able to model only materials that are composed of single elements is not adequate for many practical modeling problems. Extension of the EOF model to mixtures would bring

many more practical applications within the reach of the model. Larger length scales could be reached by the EOF model if amplitude equations were derived from it. The possibilities mentioned here are of course only a few of the many possible directions of future research for PFC models. Concerning a modeling method that has been around for less than a decade, it is obviously not very difficult to think of a handful of arguments that will drive one towards the anticipated conclusion: more research is needed.

References

[1] L. I. Rubinshtein, *The Stefan problem* (American mathematical society, United States of America, 1979)

[2] A. M. Meirmanov, *The Stefan problem* (Walter de Gruyter & Co., Berlin, 1992)

[3] J.E. Hilliard, and J.W. Cahn, Acta Met. **6**, 772 (1958)

[4] I. Steinbach, Modelling Simul. Mater. Sci. Eng. **17**, 073001 (2009)

[5] N. Provatas and K. R. Elder, *Phase-field methods in material science and engineering* (Wiley-VCH, Weinheim, 2010)

[6] F. Lindemann, Z.Phys. **11**, 609, (1910)

[7] G. Grimvall and S. Sjodin, Physica Scripta **10**, 340, (1974)

[8] J.-P. Hansen and L. Verlet, Phys. Rev. **184**, 151 (1969)

[9] Y. Singh, Phys. Rep. **207**, 351 (1991)

[10] T. V. Ramakrishnan and M. Yussouff, Phys. Rev. B **19**, 2775 (1979)

[11] Y Rosenfeld, M Schmidt, H Löwen and P Tarazona, J. Phys.: Condens. Matter **8**, L577-L581 (1996)

[12] K. R. Elder, M. Katakowski, M. Haataja and M. Grant, Phys. Rev. Lett. **88**, 245701 (2002)

[13] K. R. Elder and M. Grant, Phys. Rev. E **70**, 051605 (2004)

[14] P. Stefanovic, M. Haataja and N. Provatas, Phys. Rev. Lett. **96**, 225504 (2006)

[15] P. Stefanovic, M. Haataja and N. Provatas, Phys. Rev. E **80** 046107 (2009)

[16] J. Berry, M. Grant and K. R. Elder, Phys. Rev. E **73**, 031609 (2006)

[17] S. van Teeffelen, R. Backofen, A. Voigt and H. Lowen, Phys. Rev. E **79**, 051404 (2009)

[18] J. Berry, K. R. Elder and M. Grant, Phys. Rev. B **77**, 224114 (2008)

[19] J. Mellenthin, A. Karma and M. Plapp, Phys. Rev. B **78**, 184110 (2008)

[20] C. V. Achim, M. Karttunen, K. R. Elder, E. Granato, T. Ala-Nissila and S. C. Ying, Phys. Rev. E **74**, 021104 (2006)

[21] C. V. Achim, M. Karttunen, K. R. Elder, E. Granato, T. Ala-Nissila and S. C. Ying, J. Phys. Conference Series **100**, 072001 (2008)

[22] C. V. Achim, J. A. Ramos, M. Karttunen, K. R. Elder, E. Granato, T. Ala-Nissila, and S. C. Ying, Phys. Rev. E **79**, 011606 (2009)

[23] J. A. P. Ramos, E. Granato, S. C. Ying, C. V. Achim, K. R. Elder and T. Ala-Nissila, Phys. Rev. E **81**, 011121 (2010)

[24] K.-A. Wu, *Order-parameter models of microstructural evolution* (Ph. D thesis, Northeastern University, 2006)

[25] K.-A. Wu, A. Adland and A. Karma, Phys. Rev. E **81**, 061601 (2010)

[26] N. Goldenfeld, B. P. Athreya and J. A. Dantzig, Phys. Rev. E **72**, 020601 (2005)

[27] B. P. Athreya, N. Goldenfeld and J. A. Dantzig, Phys. Rev. E **74**, 011601 (2006)

[28] K. R. Elder, Z.-F. Huang and N. Provatas, Phys. Rev. E **81**, 011602 (2010)

[29] D.-H. Yeon, Z.-F. Huang, K. R. Elder and K. Thornton, Phil. Mag. **90**, 237 (2010)

[30] R. Spatschek and A. Karma, Phys. Rev. B **81**, 214201 (2010)

[31] Z.-F. Huang, K. R. Elder and N. Provatas, Phys. Rev. E **82**, 021605 (2010)

[32] K. R. Elder, N. Provatas, J. Berry, P. Stefanovic and M. Grant, Phys. Rev. B **75**, 064107 (2007)

[33] K-A. Wu and A. Karma, Phys. Rev. B **76**, 184107 (2007)

[34] J. Swift and P. C. Hohenberg, Phys. Rev. A **15**, 319 (1977)

[35] M. Greenwood, N. Provatas and J. Rottler, Phys. Rev. Lett. **105**, 045702 (2010)

[36] K.-A. Wu, M. Plapp and P. W. Voorhees, J. Phys.: Condens. Matter **22**, 364102 (2010)

[37] H. Lowen, J. Bechhoefer and L. S. Tuckerman, Phys. Rev. A **45**, 2399 (1992)

[38] M. Marder, Phys. Rev. A **45**, R2158 (1992)

[39] V. Tsepelin, H. Alles, A. Babkin, R. Jochemsen, A. Ya. Parshin, and I. A. Todoshchenko, Phys. Rev. Lett. **88**, 045302 (2002)

[40] U. M. B. Marconi and P. Tarazona, J. Chem. Phys. **110**, 8032 (1999)

[41] V. I. Kalikmanov, *Statistical physics of fluids* (Springer-Verlag, Berlin, 2001)

[42] J.-P. Hansen and I. R. McDonald, *Theory of simple liquids*, 3$^{\text{rd}}$ Edition (Academic, Amsterdam, 2006)

[43] T.Biben, J.-P. Hansen and J.-L. Barrat, J. Chem. Phys. **98**, 7330 (1993)

[44] W. A. Curtin and N. W. Ashcroft, Phys. Rev. A **32**, 2909 (1985)

[45] A. R. Denton and N. W. Ashcroft, Phys. Rev. A **39**, 4701 (1989)

[46] Y. Rosenfeld, Phys. Rev. Lett. **63**, 980 (1989)

[47] Y. Rosenfeld, M. Schmidt, H. Löwen, and P. Tarazona, Phys. Rev. E **55**, 4245 (1997)

[48] A. D. J. Haymet and D. Oxtoby, J. Chem. Phys. **74**, 2559 (1981)

[49] A. J. Archer and R. Evans, J. Chem. Phys. **121**, 4246 (2004)

[50] A. Jaatinen, *Applicability of the phase field crystal model in predicting phase diagrams* (Master's thesis, Helsinki University of Technology, 2006)

[51] K.-A. Wu, A. Karma, J. J. Hoyt and M. Asta, Phys. Rev. B **73**, 094101 (2006)

[52] M. I. Mendelev, S. Han, D. J. Srolovitz, G. J. Ackland, D. Y. Sun and M. Asta, Phil. Mag. A **83**, 3977 (2003).

[53] D. J. Dever, J. Appl. Phys. **43**, 3293 (1972); J. J. Adams, D. S. Agosta, R. G. Leisure and H. Ledbetter, J. Appl. Phys. **100**, 113530 (2006)

[54] Tsu Y, Takano K, 88th Spring Conf., 2-4 April **88** (Sendai: Japan Inst. Met.) p. 86 (1981); T Itami and M Shimoji, J. Phys. F: Met. Phys. **14**, L15 (1984)

[55] G. Tegze, G. Bansel, G. I. Tóth, T. Pusztai, Z. Fan and L. Gránásy, J. Comp. Phys.**228**, 1612 (2009)

[56] W. T. Read and W. Shockley,Phys. Rev. **78**, 275-289 (1950)

[57] Y. Shibuta, S. Takamoto and T. Suzuki, ISIJ Int. **48**, 1582 (2008)

[58] J-M. Zhang, Y-H. Huang, X-J. Wu, and K-W. Xu, Appl. Surf. Sci. **252**, 4936 (2005)

[59] L. E. Murr, *Interfacial Phenomena in Metals and Alloys* (Addison Wesley, New York, 1975)

[60] J. K. Percus and G. J. Yevick, Phys. Rev. **110**, 1 (1958)

[61] J. Q. Broughton, G. H. Gilmer and J. D. Weeks, Phys. Rev. B **25**, 4651 (1982)

Appendix A Semi-implicit numerical method

The numerical method that has been deployed for solving the equations of motion of the PFC models in this thesis is based on a semi-implicit operator splitting in Fourier space. Application of the method to a binary PFC model has been presented in some detail in Ref. [55]. Here we will briefly show the equations deployed for the single component case in this thesis.

First, the equation of motion for the PFC model under study is written in Fourier space as

$$\frac{\partial\hat{\psi}(\mathbf{k})}{\partial\tau} = \mathcal{L}(k)\hat{\psi}(\mathbf{k}) + \mathcal{N}\left[\hat{\psi}(\mathbf{k})\right], \tag{A.1}$$

where $\mathcal{L}$ is an operator that contains all linear parts of the equation of motion, and $\mathcal{N}$ is a non-linear operator representing the rest. For example, in the case of re-scaled SH-PFC model, i.e. Eq. (2.7), the operators are defined as

$$\mathcal{L}(k) = -k^2\left[-\epsilon + (1-k^2)^2\right] \tag{A.2}$$

and

$$\mathcal{N}\left[\hat{\psi}(\mathbf{k})\right] = -k^2\mathfrak{F}\left[\left(\mathfrak{F}^{-1}\left[\hat{\psi}(\mathbf{k})\right]\right)^3\right] \tag{A.3}$$

where $\mathfrak{F}$ and $\mathfrak{F}^{-1}$ are forward and inverse Fourier transforms. Eq. (A.1) is then discretized in k-space and time as

$$\frac{\hat{\psi}_{\mathbf{k}}^{\tau+\Delta\tau} - \hat{\psi}_{\mathbf{k}}^{\tau}}{\Delta\tau} = \mathcal{L}(k)\hat{\psi}_{\mathbf{k}}^{\tau+\Delta\tau} + \mathcal{N}\left[\hat{\psi}_{\mathbf{k}}^{\tau}\right], \tag{A.4}$$

where $\Delta\tau$ is the time step and $\mathcal{L}$ and $\mathcal{N}$ are discretized versions of the previously defined operators (i.e. continuous Fourier transforms are replaced by the discrete Fast Fourier Transforms). In Eq. (A.3) the part that is related to the linear operator $\mathcal{L}$ is evaluated implicitly at a time $\tau+\Delta\tau$, while the part that is related to $\mathcal{N}$ is evaluated explicitly at the time τ, hence the name semi-implicit operator splitting. Rearranging terms in Eq. (A.4), the final recipe for updating the field becomes

$$\hat{\psi}_{\mathbf{k}}^{\tau+\Delta\tau} = \frac{\hat{\psi}_{\mathbf{k}}^{\tau} + \Delta\tau\mathcal{N}\left[\hat{\psi}_{\mathbf{k}}^{\tau}\right]}{1-\Delta\tau\mathcal{L}(k)}. \tag{A.5}$$

The most important advantage of Eq. (A.5) over a fully explicit scheme, where also the part related to $\mathcal{L}$ is evaluated at τ rather than $\tau + \Delta\tau$, is that it is numerically much more stable. That allows one to utilize time steps that are many orders of magnitude larger than attainable in the explicit method.

ISBN 978-952-60-3518-5
ISBN 978-952-60-3519-2 (PDF)
ISSN 1795-2239
ISSN 1795-4584 (PDF)